Atmos. Chem. Phys., 22, 10077–10097, 2022
https://doi.org/10.5194/acp-22-10077-2022

Atmospheric Chemistry and Physics
Open Access
EGU

Seasonal variation in oxygenated organic molecules in urban Beijing and their contribution to secondary organic aerosol

Yishuo Guo[1], Chao Yan[1,2,3], Yuliang Liu[2], Xiaohui Qiao[4], Feixue Zheng[1], Ying Zhang[1], Ying Zhou[1], Chang Li[1], Xiaolong Fan[1], Zhuohui Lin[1], Zemin Feng[1], Yusheng Zhang[1], Penggang Zheng[5,6], Linhui Tian[7], Wei Nie[2], Zhe Wang[5], Dandan Huang[8], Kaspar R. Daellenbach[3,9], Lei Yao[1,3], Lubna Dada[3,9], Federico Bianchi[3], Jingkun Jiang[4], Yongchun Liu[1], Veli-Matti Kerminen[3], and Markku Kulmala[1,3]

[1]Aerosol and Haze Laboratory, Beijing Advanced Innovation Center for Soft Matter Science and Engineering, Beijing University of Chemical Technology, Beijing, China
[2]Joint International Research Laboratory of Atmospheric and Earth System Research, School of Atmospheric Sciences, Nanjing University, Nanjing, China
[3]Institute for Atmospheric and Earth System Research/Physics, Faculty of Science, University of Helsinki, Helsinki, Finland
[4]State Key Joint Laboratory of Environment Simulation and Pollution Control, School of Environment, Tsinghua University, Beijing, China
[5]Division of Environment and Sustainability, The Hong Kong University of Science and Technology, Hong Kong SAR, China
[6]Department of Civil and Environmental Engineering, The Hong Kong Polytechnic University, Hong Kong SAR, China
[7]Department of Civil and Environmental Engineering, Faculty of Science and Technology, University of Macau, Taipa, Macau SAR, China
[8]State Environmental Protection Key Laboratory of Formation and Prevention of Urban Air Pollution Complex, Shanghai Academy of Environmental Sciences, Shanghai, China
[9]Laboratory of Atmospheric Chemistry, Paul Scherrer Institute, Villigen, Switzerland

Correspondence: Chao Yan (chaoyan@nju.edu.cn)

Received: 6 March 2022 – Discussion started: 18 March 2022
Revised: 8 July 2022 – Accepted: 11 July 2022 – Published: 5 August 2022

Abstract. Oxygenated organic molecules (OOMs) are crucial for atmospheric new particle formation and secondary organic aerosol (SOA) growth. Therefore, understanding their chemical composition, temporal behavior, and sources is of great importance. Previous studies on OOMs mainly focus on environments where biogenic sources are predominant, yet studies on sites with dominant anthropogenic emissions, such as megacities, have been lacking. Here, we conducted long-term measurements of OOMs, covering four seasons of the year 2019, in urban Beijing. The OOM concentration was found to be the highest in summer (1.6×10^8 cm^{-3}), followed by autumn (7.9×10^7 cm^{-3}), spring (5.7×10^7 cm^{-3}) and winter (2.3×10^7 cm^{-3}), suggesting that enhanced photo-oxidation together with the rise in temperature promote the formation of OOMs. Most OOMs contained 5 to 10 carbon atoms and 3 to 7 effective oxygen atoms ($nO_{eff} = nO - 2 \times nN$). The average nO_{eff} increased with increasing atmospheric photo-oxidation capacity, which was the highest in summer and the lowest in winter and autumn. By performing a newly developed workflow, OOMs were classified into the following four types: aromatic OOMs, aliphatic OOMs, isoprene OOMs, and monoterpene OOMs. Among them, aromatic OOMs (29 %–41 %) and aliphatic OOMs (26 %–41 %) were the main contributors in all seasons, indicating that OOMs in Beijing were dominated by anthropogenic sources. The contribution of isoprene OOMs increased significantly

in summer (33 %), which is much higher than those in the other three seasons (8 %–10 %). Concentrations of isoprene (0.2–5.3 $\times 10^7$ cm^{-3}) and monoterpene (1.1–8.4 $\times 10^6$ cm^{-3}) OOMs in Beijing were lower than those reported at other sites, and they possessed lower oxygen and higher nitrogen contents due to high NO_x levels (9.5–38.3 ppbv – parts per billion by volume) in Beijing. With regard to the nitrogen content of the two anthropogenic OOMs, aromatic OOMs were mainly composed of CHO and CHON species, while aliphatic OOMs were dominated by CHON and $CHON_2$ ones. Such prominent differences suggest varying formation pathways between these two OOMs. By combining the measurements and an aerosol dynamic model, we estimated that the SOA growth rate through OOM condensation could reach 0.64, 0.61, 0.41, and 0.30 µg m^{-3} h^{-1} in autumn, summer, spring, and winter, respectively. Despite the similar concentrations of aromatic and aliphatic OOMs, the former had lower volatilities and, therefore, showed higher contributions (46 %–62 %) to SOA than the latter (14 %–32 %). By contrast, monoterpene OOMs and isoprene OOMs, limited by low abundances or high volatilities, had low contributions of 8 %–12 % and 3 %–5 %, respectively. Overall, our results improve the understanding of the concentration, chemical composition, seasonal variation, and potential atmospheric impacts of OOMs, which can help formulate refined restriction policy specific to SOA control in urban areas.

1 Introduction

Atmospheric aerosols affect global climate both directly and indirectly (Stocker, 2014) and are known to have a detrimental influence on human health (Lelieveld et al., 2015). Modeling studies have suggested that new particle formation (NPF) dominates the number concentration of particles and is an important contributor to cloud condensation nuclei (CCN) in the global atmosphere (Merikanto et al., 2009; Gordon et al., 2017). In terms of aerosol mass, it has been shown that a significant fraction is composed of secondary organic aerosol (SOA; Zhang et al., 2007; Jimenez et al., 2009; Hallquist et al., 2009). In both NPF and SOA formation processes, oxygenated organic molecules (OOMs; see the definition in Sect. S2 the work of Nie et al., 2022) have been acknowledged as an important contributor, and thus, advanced understanding of OOMs is crucial.

The role of OOMs in NPF was first suggested in 2002, but they could not be identified or quantified at that time (O'Dowd et al., 2002). Then, the emergence of the atmospheric pressure interface time-of-flight (APi-ToF) mass spectrometer (Junninen et al., 2010; Ehn et al., 2010, 2012) and chemical ionization-APi-ToF (CI-APi-ToF) mass spectrometer (Jokinen et al., 2012; Ehn et al., 2014) provided the first direct measurement of highly oxygenated organic molecules (HOMs), a subgroup of OOMs with the most oxygen content, which inspired later studies on their role in NPF and SOA growth (Kulmala et al., 2013; Schobesberger et al., 2013; Riccobono et al., 2014; Ehn et al., 2014; Kirkby et al., 2016; Tröstl et al., 2016; Bianchi et al., 2016; Lehtipalo et al., 2018; Rose et al., 2018; Stolzenburg et al., 2018; Mohr et al., 2019; Heinritzi et al., 2020; Yan et al., 2020; Caudillo et al., 2021). These studies found that the functionality and volatility of OOMs are the key factors in determining whether OOM species can participate in NPF (Donahue et al., 2013). More specifically, ultra low volatility organic compounds (ULVOCs; whose mass saturation concentrations, C^*, are smaller than 3×10^{-9} µg m^{-3} or whose number saturation concentrations, N^*, are smaller than 6 cm^{-3}, by assuming an average molar mass of 300 Da) are the main participator of the initial nucleation at certain conditions (Schervish and Donahue, 2020), and extremely low volatility organic compounds (ELVOCs; $3 \times 10^{-9} < C^* < 3 \times 10^{-4}$ µg m^{-3} and $6 < N^* < 6 \times 10^5$ cm^{-3}) and low volatility organic compounds (LVOCs; $3 \times 10^{-4} < C^* < 0.3$ µg m^{-3} and $6 \times 10^5 < C^* < 6 \times 10^8$ cm^{-3}) can have a dominant contribution to the growth of newly formed particles.

Owing to the significance of OOMs in atmospheric aerosol formation and growth, its reliable measurement is of high importance. Up until now, the majority of reported sites in the lower troposphere with OOM measurement are non-urban areas, such as forest, agricultural pasture, and countryside, where the most abundant OOM species are oxidized products from monoterpenes and isoprene. In the boreal forest of southern Finland, the reported OOM concentration was the highest in summer (4.6×10^8 cm^{-3}; Huang et al., 2021), followed by autumn (8.0×10^7 cm^{-3}; Zha et al., 2018) and spring ($\sim 4.0 \times 10^7$ cm^{-3}; Yan et al., 2016; Roldin et al., 2019; Bianchi et al., 2017). The level of OOMs also varied significantly at different sites. In Melpitz agricultural forest of central Europe, the OOM concentration (2.5×10^8 cm^{-3} in summer; Mutzel et al., 2015) was comparable with that in Hyytiälä, while in the Alabama forest of the United States, the OOM concentration was much higher (4.8×10^9 cm^{-3} in summer; Massoli et al., 2018; Krechmer et al., 2015), possibly due to higher UVB (type B ultraviolet) and temperature. Besides, monoterpene OOMs at agricultural–rural mixed Vielbrunn were also detected (3.6×10^6 cm^{-3} in spring), and results showed that many other unidentified species also took a large fraction, especially at night (Kürten et al., 2016). All of these studies highlight the importance of OOM measurement worldwide. Several urban observations were also reported (Brean et al., 2019; Ye et al., 2021). Although they

showed that OOMs in Chinese urban cities contain a significant fraction of compounds with six to nine carbons, and that many contain nitrogen, they either reported concentrations of a few chosen species or just spectral signals. Moreover, due to the limitation of short measurement periods, they were incapable of exploring the seasonal behavior of OOM concentration and detailed composition, which are crucial for fully evaluating their potential contribution to the growth of SOA.

In this work, we studied the OOMs measured by a CI-APi-ToF mass spectrometer using nitrate (NO_3^-) as the reagent ions. The dataset covers four seasons of year 2019. We performed detailed molecular analyses within the mass-to-charge ratio between 200–400 Th and identified around 1000 OOMs for each season. The seasonal variations in their concentration, molecular composition, volatility distribution, and potential SOA contribution were systematically investigated for the first time. Furthermore, with a newly developed workflow, we traced their potential sources, including aromatics, aliphatics, monoterpenes, and isoprene. Finally, we evaluated the relative contribution of anthropogenic and biogenic sources in different seasons.

2 Measurements and methods

2.1 Measurements

The measurement was conducted at the west campus of the Beijing University of Chemical Technology (39.95° N, 116.31° E) on the fifth floor of the teaching building, which is about 15 m a.g.l. (above ground level). This station is a representative urban site, and a detailed description can be found elsewhere (Liu et al., 2020; Yan et al., 2021; Guo et al., 2021).

The concentration of OOMs was measured by a nitrate (NO_3^-)-CI-APi-ToF mass spectrometer (abbreviated as nitrate CIMS; Aerodyne Research, Inc.). The basic working principle of this instrument can be found elsewhere (Jokinen et al., 2012), and the detailed sampling configuration is the same as that reported by Yan et al. (2021). There were two steps included in the quantification of OOM concentration. First, a mass-dependent transmission experiment was conducted according to a previous study (Heinritzi et al., 2016), and the transmission curve was obtained by comparing the decrease in primary ion signals and the increase in added perfluorinated acid signals. Second, the calibration factor of sulfuric acid was applied to estimate OOM concentration. Some studies have shown that OOM molecules with a lower oxygen number are not ionized as efficiently as sulfuric acid by NO_3^- (Hyttinen et al., 2015, 2018; Riva et al., 2019). Therefore, the reported OOM concentration in this study should be regarded as the lower limit. The concentration of each OOM molecule can be calculated as follows:

$$[\mathrm{OOM}] = \frac{\sum_{i=0}^{1}(\mathrm{OOM}t)(\mathrm{HNO_3})_i\mathrm{NO_3^-} + (\mathrm{OOM}-\mathrm{H})^-(\mathrm{HNO_3})_i}{\sum_{i=0}^{2}(\mathrm{HNO_3})_i\mathrm{NO_3^-}} \times C/T_{\mathrm{OOM}}. \quad (1)$$

The numerator on the right-hand side is the sum of detected signal of that OOM in the unit of counts per second (cps), either as a cluster of a neutral molecule combined with NO_3^-, $(OOM)(HNO_3)_iNO_3^-$, or as a deprotonated ion, $(OOM\text{-}H)^-$. It should be pointed out that, in the nitrate CIMS, most OOMs were detected as being the cluster form of $(OOM)NO_3^-$, and detailed information can be found in Sect. S1 in the Supplement. The denominator is the sum of all reagent ion signals in cps. C is the calibration factor of sulfuric acid ranged from 6.07×10^9 to 7.47×10^9 cm^{-3}/ (normalized cps) during the whole year. Such a narrow range of the calibration factor also indicated that our instrument had a stable performance during the measurement period. T_{OOM} is the relative transmission efficiency of a specific OOM molecule in comparison with that of the reagent ions.

The number concentration of aerosol particles from 6 to 840 nm was measured by a differential mobility particle sizer (DMPS; Aalto et al., 2001). The mass concentration of $PM_{2.5}$ was measured with a tapered element oscillating microbalance dichotomous ambient particulate monitor (TEOM 1405-DF; Thermo Fisher Scientific Inc, USA). The chemical composition of the $PM_{2.5}$ was obtained from an aerosol chemical speciation monitor (ACSM; Jayne et al., 2000; Drewnick et al., 2005), and positive matrix factorization (PMF) analysis was further performed to separate secondary organic aerosols from primary ones. Meteorological parameters were measured with a weather station (AWS310; Vaisala) located on the rooftop of the building. Concentrations of trace gases, including carbon monoxide (CO), sulfur dioxide (SO_2), nitrogen oxides (NO_x), and ozone (O_3), were monitored using Thermo Environmental Instruments (models 48i, 43i-TLE, 42i, and 49i, respectively).

The measurement period covers four seasons of the year 2019, including 135 d in total. Winter, spring, summer, and autumn periods range from 5 January to 14 February, 15 March to 14 April, 10 July to 9 August, and 19 October to 18 November, respectively.

2.2 A revised workflow for the classification of OOM sources

A recently developed workflow, based on the molecular composition and the up-to-date knowledge of atmospheric OOM formation chemistry, was used for retrieving their possible sources (Xu et al., 2021; Nie et al., 2022). In this approach, mass spectral binning combined with positive matrix factorization (binPMF; Zhang et al., 2019) needs to be performed first to extract the factor of monoterpene OOMs. However, as

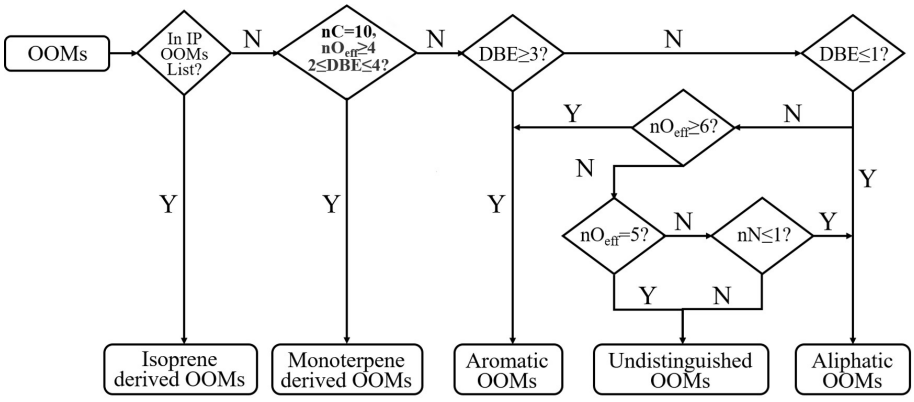

Figure 1. Workflow for retrieving OOM sources. IP OOMs represents isoprene-derived OOMs. nO_{eff} and nN are the numbers of effective oxygen and nitrogen in each OOM molecule, respectively. Y and N denote yes and no, respectively.

performing binPMF is time-consuming and not suitable for large datasets as used in this study, we replaced the binPMF step by the criteria of $nC = 10$, $nO_{eff} \geq 4$, and $2 \leq DBE \leq 4$ (Fig. 1) for the selection of monoterpene OOMs. Such standards were set based on their reported composition (Ehn et al., 2012; Yan et al., 2016; Jokinen et al., 2014; Boyd et al., 2015; Berndt et al., 2016, 2018). Here, nC is the carbon number. nO_{eff} ($= nO - 2 \times nN$) is the effective oxygen number, which subtracts the number of oxygen bonded to nitrogen by assuming that all nitrogen atoms are in the form of nitrate groups ($-ONO_2$) or peroxynitrate nitrate group ($-OONO_2$). To our best knowledge, this is the common case for all nitrogen-containing compounds formed through the reaction between RO_2 and NO_x (Orlando and Tyndall, 2012; Seinfeld and Pandis, 2016). Exceptions are those nitrophenols (Yan et al., 2016; Wang et al., 2019; Song et al., 2021) that were classified separately (Nie et al., 2022). The reason for choosing nO_{eff} rather than nO is that it better reflects the oxidation state of closed-shell molecules and their parent RO_2 radicals. For example, $C_7H_9O_5$ peroxy radical can produce both $C_7H_{10}O_4$ and $C_7H_9O_6N$ when reacting with NO, and all of them have the same nO_{eff} of four. In addition, nO_{eff} considers the influence of nitrogen and represents volatility more directly (Yan et al., 2020) and, thus, makes it easier for the volatility comparison among OOMs with different nitrogen atoms.

DBE denotes the double bond equivalence and is calculated as $2\,nC + 2 - nH - nN)/2$, which is the same as the term degree of unsaturation. The DBE of one OOM molecule is influenced by both its precursor and the oxidation processes. For example, aromatic volatility organic compounds (VOCs) have DBE values no smaller than 4. For their oxidation products, a previous study has shown that, under OH exposures equivalent to approximately 10 h to 15 d in typical atmospheric conditions, they possess DBE values no smaller than 2 (Garmash et al., 2020). However, reported monoterpene OOMs also have DBE values the same as aromatic OOMs, which makes them difficult to distinguish. According to laboratory studies, the majority of monomer products from monoterpene oxidation are C10 compounds (Yan et al., 2020). Measurement results also showed that the concentrations of C10 aromatic VOCs are very low (Zhang et al., 2017) compared with other C6–C9 ones. Therefore, those C10 OOMs with DBE values of 2 to 4 are likely monoterpene OOMs. For OOMs with DBE values smaller than 2, neither aromatics nor monoterpene oxidation could explain their formation. Hence, the precursors of those OOMs should be the ones without aromatic rings and have smaller DBE values, such as alkanes, alkenes, and some unsaturated oxygen-containing VOCs (OVOCs). OOMs with DBE values of 2 are rather complex. Their precursors could be aromatics, aliphatics, or other unknown sources, and a detailed discussion of the classification criteria can be found in Nie et al. (2022).

Due to the complexity of atmosphere, there indeed remain some uncertainties in the workflow. For example, a recent study found that some aliphatic VOCs were able to produce OOMs with DBE values of 2–3 and nO_{eff} no smaller than 6 (Wang et al., 2021), which, however, are classified as aromatic OOMs in the workflow. Nie et al. (2022) have tested the performance of the workflow on OOMs from Wang et al. (2021). Results show that the accuracy is almost 100 % for OOMs from *n* decane and ∼ 75 % for OOMs from cyclohexane (Nie et al., 2022). Thus, the workflow is generally reliable in classifying aliphatic OOMs. In addition, the VOC-to-NO_x ratios in the experiments of Wang et al. (2021; Table S17) is much higher than in urban Beijing (Table S18). This high level of NO_x might suppress the autoxidation as the $RO_2 + NO$ termination reaction likely dominates the fate of RO_2 radicals, leading to comparatively lower nO_{eff}. In this way, aliphatic OOMs find it difficult to reach nO_{eff} of 6. The revised workflow finally divided OOMs into the following five groups: isoprene (IP) OOMs, monoterpene (MT) OOMs, aromatic OOMs, aliphatic OOMs, and a small number of undistinguished OOMs (6 %–9 %) that cannot be classified into those four types.

Table 1. Mean, standard deviation (SD), median, and 25 and 75 percentiles (25th and 75th) of measured OOM concentrations at various lower tropospheric sites.

Measurement site	Period	Mean (cm^{-3})	SD (cm^{-3})	Median (cm^{-3})	25th (cm^{-3})	75th (cm^{-3})	Reference
Beijing, China	Jan–Feb 2019	2.7×10^7	1.7×10^7	2.3×10^7	1.3×10^7	3.6×10^7	This study
Beijing, China	Mar–Apr 2019	6.9×10^7	5.1×10^7	5.7×10^7	3.1×10^7	8.9×10^7	This study
Beijing, China	Jul–Aug 2019	1.6×10^8	7.5×10^7	1.6×10^8	1.1×10^8	2.2×10^8	This study
Beijing, China	Oct–Nov 2019	8.3×10^7	5.2×10^7	7.9×10^7	4.0×10^7	1.2×10^8	This study
Hong Kong SAR, China	Nov 2018	2.3×10^8	1.1×10^8	2.1×10^8	1.5×10^8	2.9×10^8	Nie et al. (2022)
Shanghai, China	Nov 2018	7.8×10^7	6.3×10^7	6.1×10^7	2.6×10^7	1.2×10^8	Nie et al. (2022)
Nanjing, China	Nov 2018	7.7×10^7	5.4×10^7	7.2×10^7	3.1×10^7	1.1×10^8	Nie et al. (2022)
Hyytiälä forest, Finland	Apr–May 2012	7.5×10^7	6.1×10^7	5.7×10^7	3.6×10^7	9.2×10^7	Yan et al. (2016)
Hyytiälä forest, Finland	May 2013	1.4×10^7	7.9×10^6	1.2×10^7	8.1×10^6	1.8×10^7	Roldin et al. (2019)
Hyytiälä forest, Finland	Apr–Jun 2013	4.5×10^7	1.2×10^7	4.9×10^7	3.2×10^7	5.5×10^7	Bianchi et al. (2017)
Hyytiälä forest, Finland	Sep 2016	1.2×10^8	1.0×10^8	8.0×10^7	3.8×10^7	1.7×10^8	Zha et al. (2018)
Melpitz, Germany	Jul 2013	2.7×10^8	1.7×10^8	2.5×10^8	1.4×10^8	3.5×10^8	Mutzel et al. (2015)
Alabama forest, USA	Jun–Jul 2013	4.7×10^9	1.5×10^9	4.8×10^9	3.7×10^9	5.3×10^9	Massoli et al. (2018)

3 Results and discussions

3.1 Seasonal variation in OOM concentration and composition

The concentration and molecular composition are the most fundamental characteristics of OOMs. We summarized the OOM concentrations in Beijing and other lower tropospheric sites in Table 1 and Fig. 2 for better comparison. Generally, a clear seasonal trend of OOM concentration in Beijing can be observed, where total OOM concentration is highest in summer (1.6×10^8 cm^{-3}), followed by autumn (7.9×10^7 cm^{-3}) and spring (5.7×10^7 cm^{-3}), and the lowest in winter (2.3×10^7 cm^{-3}). This apparent increase in OOM concentrations with an increased temperature and theoretical global radiation indicates that elevated solar radiation along with higher temperature favors the generation of OOMs. In comparison to other locations, the level of OOMs in urban Beijing varied within the ranges of previously reported ones (Yan et al., 2016; Roldin et al., 2019; Bianchi et al., 2017; Zha et al., 2018; Huang et al., 2021; Mutzel et al., 2015; Massoli et al., 2018; Nie et al., 2022). Interestingly, the above clear correlation between global radiation (or temperature) and OOM concentration can also be seen in other locations, yet OOMs in forest environments are, in general, higher than in urban or suburban areas. On the one hand, this observation suggests that OOM formation at a specific environment is prevailingly influenced by the strength of atmospheric photochemistry; on the other hand, the forest environment appears to have more abundant OOMs than urban environments, possibly because the OOM yield of biogenic VOCs is higher than that of anthropogenic VOCs (Berndt et al., 2016; Teng et al., 2017; Garmash et al., 2020; Molteni et al., 2018). Yet, a quantitative explanation of the OOM variation between seasons and locations requires comprehensive measurements and analyses on both the production and loss of OOMs.

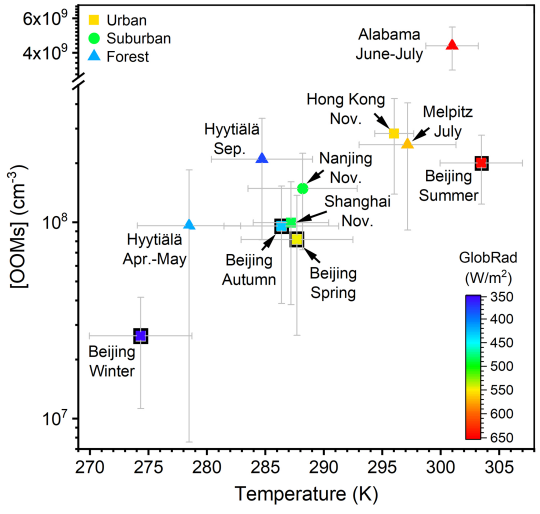

Figure 2. OOM concentration vs. temperature at various lower tropospheric sites during the daytime (07:00–17:00 LT). Data points are colored by theoretical global radiation (GlobRad). Square, circle, and triangle markers represent urban, suburban, and forest areas, respectively. The gray error bars show standard deviations (1σ). Nanjing, Shanghai, and Hong Kong SAR datasets are from Nie et al. (2022), Melpitz data are from Mutzel et al. (2015), Alabama data are from Massoli et al. (2018), and Hyytiälä datasets are from Yan et al. (2016) and Zha et al. (2018).

To further demonstrate the seasonal influence of solar radiation and precursor VOCs on OOM concentration, we classified OOMs of each season into four groups based on the brightness parameter (Dada et al., 2017) and $PM_{2.5}$ level, respectively. As shown in Fig. S6, in seasons other than sum-

Table 2. Main CHO, CHON, and $CHON_2$ OOM species measured in this study.

DBE	CHO OOMs	CHON OOMs	$CHON_2$ OOMs
0	$C_nH_{2n+2}O_6$	$C_nH_{2n+1}O_{3-8}N$	$C_nH_{2n}O_{4-11}N_2$
1	$C_nH_{2n}O_{2-8}$	$C_nH_{2n-1}O_{3-9}N$	$C_nH_{2n-2}O_{4-10}N_2$
2	$C_nH_{2n-2}O_{3-7}$	$C_nH_{2n-3}O_{3-9}N$	$C_nH_{2n-4}O_{5-11}N_2$
3	$C_nH_{2n-4}O_{2-8}$	$C_nH_{2n-5}O_{3-10}N$	$C_nH_{2n-6}O_{8-11}N_2$
4	$C_nH_{2n-6}O_{3-9}$	$C_nH_{2n-7}O_{3-9}N$	$C_nH_{2n-8}O_{7,8}N_2$
5	$C_nH_{2n-8}O_{3-8}$	$C_nH_{2n-9}O_{4-10}N$	$C_nH_{2n-10}O_{6-10}N_2$

mer, OOM concentration under polluted conditions is much higher than that under clean conditions, which likely results from the elevation of precursors coming along with polluted air masses and the accumulation during the pollution. Besides, the concentration of total OOMs on sunny days is higher than that on cloudy days, implying that photochemical oxidation plays a key role in the production of OOM molecules. There is one exception that OOM concentration is not significantly different between sunny and cloudy days under clean conditions in autumn, and the cause cannot be concluded in this study without a complete VOC measurement.

For OOM composition, the two-dimensional H/C-O_{eff}/C (ratio of hydrogen number to carbon number vs. ratio of effective oxygen number to carbon number) diagrams are plotted to show their characteristics (Fig. S7). And the main CHO, CHON, and $CHON_2$ OOM species are also summarized in Table 2. Generally, the composition of OOM molecules exhibits a high similarity among different seasons, suggesting no significant changes in OOM formation in general. However, two seasonal characteristics can be found. First, the most oxygenated OOM molecules, such as $C_nH_{2n-2}O_{6,7}$, $C_nH_{2n-4}O_{7,8}$, $C_nH_{2n+1}O_8N$, and $C_nH_{2n-1}O_9N$ OOMs, are mainly observed in summer, and meanwhile, the least oxygenated ones, e.g., $C_nH_{2n-7}O_2N$ and $C_nH_{2n-9}O_{4,5}N$, are mostly detected in winter. These observations indicate that, in addition to the enhanced OOM concentration, strong photochemistry also leads to a high oxidation state of OOM. And these summer-specific OOMs can be classified as highly oxygenated organic molecules (HOMs). Second, $C_5H_{10}O_8N_2$ is exceedingly high in summer. A previous study suggested that $C_5H_{10}O_8N_2$ is one dominant oxidation product from isoprene (Xu et al., 2021), and therefore, the high concentration of $C_5H_{10}O_8N_2$ is a clear indication of intensive isoprene oxidation in summer, which will be discussed in detail in Sect. 3.2.

For a better understanding of OOM composition variation among seasons, the distributions of nC, nO_{eff}, nN, and DBE, as well as their seasonal variations, are further analyzed. It should be pointed out that the concentration (5.3×10^7 cm^{-3}) and the fraction (33 %) of IP OOMs in summer is much higher than those in other three seasons, and therefore, they are plotted in bars with diagonal lines individually (Fig. 3). In terms of carbon content, the majority of OOMs contain 5 to 10 carbon atoms. For OOMs with 6 to 10 carbon atoms, in seasons other than summer, C6 are the most abundant, and a decreasing trend can be seen along with increasing nC, while in summer, an opposite trend is observed, i.e., the relative contribution increases with an increasing nC. The causes behind the different trends in summer and other seasons are complex but might include changes in the precursor VOC distribution, varying reactivity responses of VOCs to temperature, and the volatilities of OOMs that influence their atmospheric lifetime. Further analysis on this topic will be made in the future. For C5 OOMs, the contribution from isoprene varies from less than half in winter and spring to $\sim$ 70 % in summer. The high contribution of IP OOMs in summer is in line with the strong isoprene emission coupled with the enhanced photo-oxidation (Cheng et al., 2018; Zhang et al., 2020).

Concerning the oxygen content, most OOMs contain three to seven effective oxygen atoms, accounting for 86 %–95 % of total OOMs in all seasons. With the increase in the effective oxygen number, the contribution of corresponding OOMs first increases and then decreases, with $nO_{eff} = 4$ OOMs having the highest fraction. Figure S8 shows that the concentration-weighted average nO_{eff} is the highest in summer and lowest in winter and autumn, which is consistent with the observation of individual molecules, where the most highly oxygenated ones are usually more abundant in summer. The enhanced multi-step oxidation (Garmash et al., 2020; Wu et al., 2021) and favored auto-oxidation (Molteni et al., 2018; Wang et al., 2017; S. Wang et al., 2018; Bianchi et al., 2019) at high temperatures in warmer seasons are most likely the causes. Furthermore, when taking IP OOMs into account, $nO_{eff} = 4$ becomes even more prominent in summer, in which $C_5H_{10}O_8N_2$ takes the largest portion and accounts for 77 % of $nO_{eff} = 4$ IP OOMs. In winter and autumn, however, $nO_{eff} = 3$ has a much higher fraction than those in the other two seasons, and those OOMs are mainly composed of low-DBE compounds, such as $C_nH_{2n}O_7N_2$, $C_nH_{2n-2}O_7N_2$, and $C_nH_{2n-1}O_5N$ species.

As for the nitrogen content, the vast majority (98 %–99 %) of OOMs contain zero to two nitrogen atoms, in which CHON OOMs take the largest fraction, varying from 42 % to 51 % among seasons. It should be noted that, although the mixing ratios of NO_x in different seasons change significantly, the nitrogen distributions of non-isoprene OOMs are similar, which is probably due to the fact that NO (0.6–10.0 ppbv – parts per billion by volume) and NO_2 (8.9–28.3 ppbv) concentrations in urban Beijing are always high throughout the year. Those nitrogen atoms could come from either NO_3 radical oxidation or NO_x termination. During the day, nitrogen is likely added mainly through NO_x termination, as the NO_3 radical should be photolyzed or titrated by NO. However, in the absence of NO_3 photolysis at night, when the NO concentration is low, the concentration of NO_3 radical could reach up to $\sim$ 10 pptv (parts per trillion by

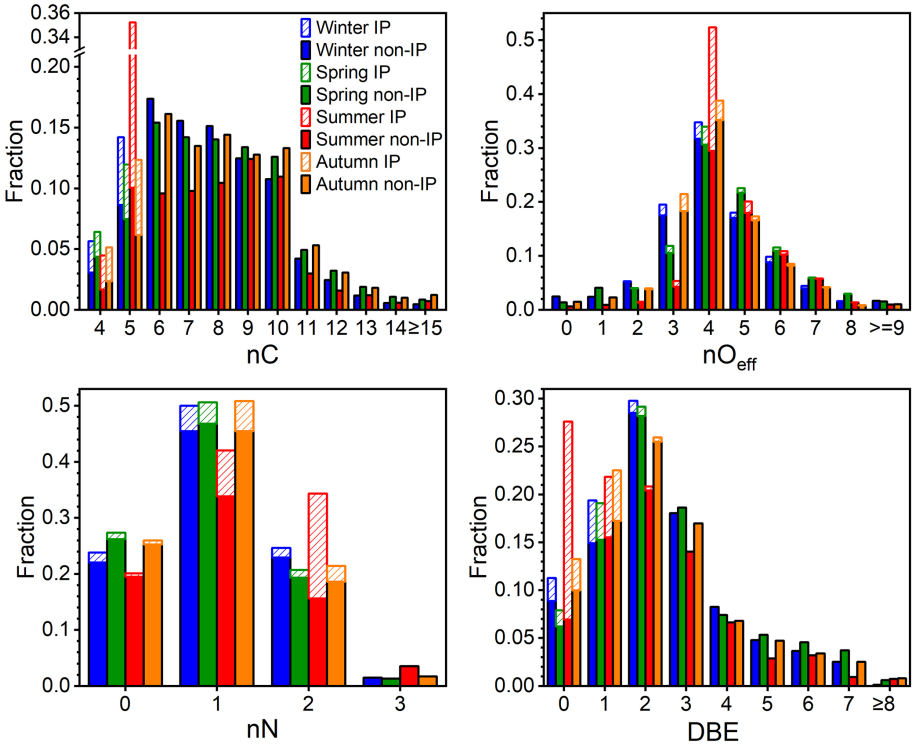

Figure 3. The number of carbon (nC), effective oxygen (nO$_{eff}$), nitrogen (nN), and double bond equivalence (DBE) distributions of OOMs for four seasons. The abbreviations IP and non-IP represent IP OOMs and other non-isoprene OOMs, respectively. The bars with diagonal lines and filled colors represent IP OOMs and non-isoprene OOMs, respectively.

volume; 2.7×10^8 cm^{-3}) in Beijing (H. Wang et al., 2018). Under such levels, the NO_3 radical could even dominate the oxidation of biogenic VOCs (i.e., isoprene and monoterpenes) and some aliphatic VOCs, yet the oxidation of aromatic VOCs are driven by OH radicals (Tables S4 and S5). Therefore, nitrogen is possibly added through both processes at night.

In the case of DBE distribution, most OOMs comprise 0 to 6 DBE values, and there is not too much difference among seasons for non-isoprene OOMs. Generally, with the increase in DBE, the fraction of corresponding non-isoprene OOMs first increases and then decreases, with DBE = 2 OOMs having the highest contribution (20 %–29 %). And this is possibly caused by the fact that almost all precursor VOCs, such as aromatics, aliphatics, and monoterpenes, can form oxidation products with DBE value of 2. OOMs with DBE larger than 4 and nC no smaller than 10 are likely derived from polycyclic aromatic hydrocarbons (PAHs; DBE $\geq$ 7), and their fraction varies from 5 % in summer to 7 %–8 % in the other three seasons. This demonstrates that PAHs may also have a non-negligible contribution to total OOMs. For IP OOMs, most of them possess 0 or 1 DBE, and only a small fraction (2 %–16 %) of them retains the DBE of precursor isoprene. This indicates that hydroxyl or hydroperoxyl are the major functional groups of these products, whereas products with higher DBE values are not prominent. It could mean that compounds containing carbonyl or epoxide groups are either not efficiently formed under the urban environment or lost fast via heterogeneous reactions (Riedel et al., 2015; Zhang et al., 2022). Meanwhile, the instrumental detection bias, i.e., nitrate CIMS being less sensitive to carbonyl and epoxide groups, cannot be excluded. Therefore, further combinations of CIMS instruments with different chemical ionization methods are highly desirable in the future.

3.2 Characteristics of source-classified OOMs

With the workflow described in Sect. 2.2, total OOMs were classified into the following four types: IP OOMs, MT OOMs, aromatic OOMs, and aliphatic OOMs. As shown in Fig. 4, the seasonal concentrations of OOMs from different sources vary with the same trend and are highest in summer, followed by autumn, spring, and winter. During the whole year, aromatic OOMs (29 %–41 %) and aliphatic OOMs (26 %–41 %) are the most abundant categories, demonstrating that OOMs in Beijing are dominantly from anthropogenic sources. This is also consistent with the observation of SOA composition in previous studies (Le Breton et al., 2018; Mehra et al., 2021). In terms of OOMs from biogenic sources, IP OOMs show a prominent contribution in summer (33 %), which is much higher than in other seasons (8 %–10 %). Although it has recently been suggested that isoprene

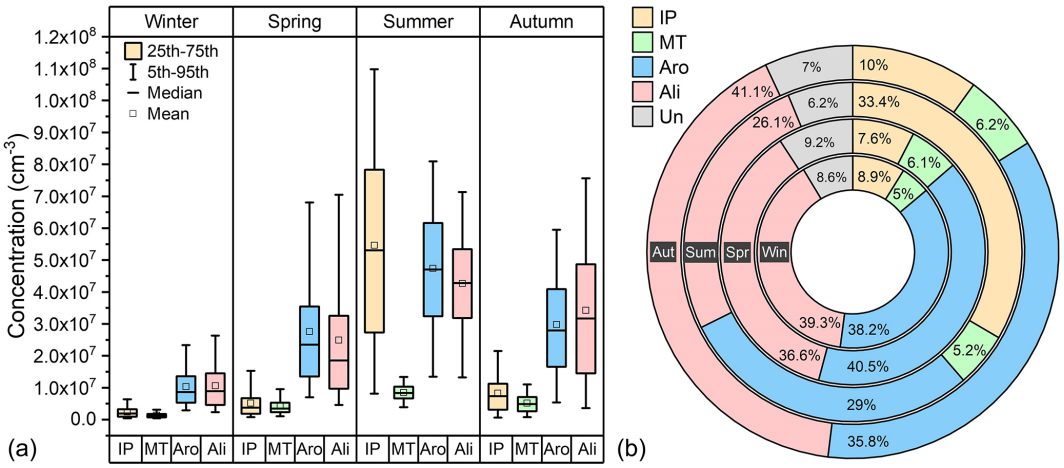

Figure 4. Concentration **(a)** and fraction **(b)** of source-classified OOMs in four seasons. The abbreviations IP, MT, Aro, Ali, and Un stand for IP OOMs, MT OOMs, aromatic OOMs, aliphatic OOMs and undistinguished OOMs, respectively. Win, Spr, Sum, and Aut represent winter, spring, summer, and autumn, respectively.

can have both biogenic and anthropogenic sources (Wagner and Kuttler, 2014; Panopoulou et al., 2020), the much higher enhancement of IP OOMs in summer can only be explained by the large additional biogenic emission (Cheng et al., 2018; Mo et al., 2018). For MT OOMs, however, the fractional contribution does not show a seasonal variation which is as clear as that of IP OOMs – it only varies between 5 % and 6 %.

3.2.1 Characteristics of biogenic OOMs

The spectral profiles and the fractions of IP OOMs with different nitrogen numbers in four seasons are shown in Fig. 5. Prominent IP OOM species include $C_4H_6O_4$, $C_5H_8O_4$, $C_4H_7O_{6,7}N$, $C_5H_9O_{5-7}N$, $C_5H_{10}O_{7,8}N_2$, and $C_5H_9O_{10}N_3$. $CHON_3$ OOM ($C_5H_9O_{10}N_3$) is detected in all four seasons, suggesting that multi-generation oxidation is involved throughout the year. Besides, the composition of IP OOMs exhibits a clear seasonal variation. First, compared with other three seasons, $C_5H_{10}O_8N_2$ and $C_5H_9O_{10}N_3$ have much higher contributions in summer, indicating that NO_x may be involved more efficiently in the oxidation process of isoprene despite its lower concentration (Fig. S10 and Table S1 in the Supplement). In addition, nighttime NO_3 radicals produced efficiently during summer nights (H. Wang et al., 2018) should also promote their formation. Second, despite the overall lowest concentrations of IP OOMs in winter, $C_4H_8O_7$ exhibits a maximum concentration (Fig. S9) and the highest fraction, implying that it may have additional sources, other than isoprene oxidation, in winter. Third, due to the influence of $C_5H_{10}O_8N_2$ and $C_5H_9O_{10}N_3$, $CHON_2$ and $CHON_3$ IP OOMs take an extremely large proportion (~ 67 %) in summer. And, interestingly, the seasonal trend of nitrate IP OOM fraction (from largest to smallest is summer, autumn, spring, and winter) did not follow the variation in NO_x concentration (from highest to lowest is autumn, winter, spring, and summer; Fig. S5 and Table S1), which suggests that the formation of nitrate IP OOMs probably has a non-linear response to NO_x.

The concentrations of these prominent IP OOM molecules during summertime in Beijing, Nanjing (32.12° N, 118.95° E; Liu et al., 2021), and Alabama mixed forest (32.90° N, 87.25° W; Krechmer et al., 2015; Massoli et al., 2018) are further compared (Fig. 6). Please note that these molecules plotted are not all the IP OOMs but rather selected abundant ones reported in the literature and in this study. As shown in Fig. 6a, IP OOMs exhibit the highest concentration in the Alabama forest and the lowest one in Beijing, and the level of IP OOMs in Beijing and Nanjing is comparable. This concentration difference is likely caused by the variation in biogenic isoprene emissions, since the Alabama measurement was conducted in a forest, the Nanjing site is a suburban area with large vegetation coverage nearby, and the Beijing site is located in an urban downtown area. Besides, the overall varying patterns of IP OOM species in Beijing and Nanjing are very similar, indicating that isoprene in those two urban sites undergo similar oxidation pathways. In terms of oxygen distribution, Beijing and Nanjing are rather similar in that $nO_{eff} = 4$ OOMs contribute the most, whereas in Alabama, $nO_{eff} = 5$ ones are the most abundant (Fig. 6b). This lower oxygen content in urban cities is probably caused by the high NO_x levels (11.1, 8.5, and 0.5 ppbv for Beijing, Nanjing, and Alabama, respectively; Fig. S10), since NO_x efficiently suppresses the oxygen addition of RO_2 radicals (Zhao et al., 2018). Furthermore, the different NO_x levels among the three sites also influence the nitrogen content that Beijing is the highest and Alabama is the lowest (Fig. 6c).

From the perspective of diurnal variation, CHO IP OOMs in Beijing possess one daytime peak, while CHON OOMs mainly contain a day–night dual-peak type or nocturnal-

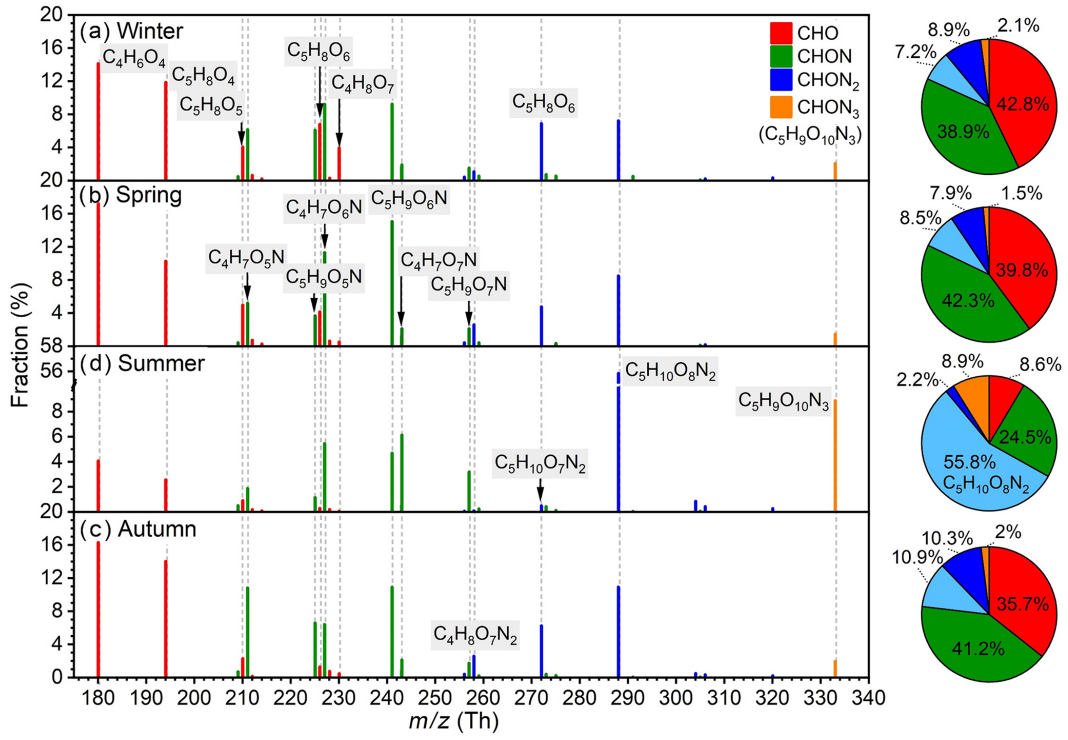

Figure 5. Fractional profiles of each IP OOM molecule in **(a)** winter, **(b)** spring, **(c)** summer, and **(d)** autumn. The mass-to-charge ratio (m/z) denotes OOM clustered with NO_3^- or as deprotonated ones. The fraction of each compound is calculated as the ratio of its concentration to the total concentration of IP OOMs. The red, green, blue, and orange bars are for CHO, CHON, $CHON_2$, and $CHON_3$ OOMs, respectively. Please note that $CHON_3$ OOMs only include $C_5H_9O_{10}N_3$.

peak-only type (Fig. S11), which is similar to that reported in the Alabama forest (Massoli et al., 2018). But it should be noted that the diurnal variations in some CHON IP OOMs with same molecular composition in this study and Massoli et al. (2018) are not identical, suggesting that their formation pathways are different under various atmospheric conditions.

Different from IP OOMs, the overall composition distributions of MT OOMs in the four seasons are quite similar and vary with identical oxygen addition patterns (Fig. 7). Predominant MT OOM molecules are $C_{10}H_{14}O_{4–8}$, $C_{10}H_{16}O_{4\text{-}6}$, $C_{10}H_{18}O_{4,5}$, $C_{10}H_{13,15,17}O_{6\text{-}9}N$ and $C_{10}H_{14,16}O_{8–10}N_2$. Besides, most MT OOMs belong to CHON category (54 %–59 %) and the CHO (18 %–21 %) and $CHON_2$ (19 %–27 %) ones, with a comparable contribution during the year.

Then, for a better understanding of MT OOM characteristics under different atmospheric environments, representative MT OOM molecules in summer Beijing, spring Hyytiälä forest (61.8° N; Yan et al., 2016), and summer Alabama mixed forest (Massoli et al., 2018) are further compared. The following differences can be identified. First, MT OOM concentrations are the highest in Alabama and the lowest in urban Beijing (Fig. 8a), which should result from the synergetic influence of UVB, temperature, and precursor monoterpenes. Second, the levels of the two MT radicals that have high concentrations in the Hyytiälä forest, $C_{10}H_{15}O_8\bullet$ and $C_{10}H_{15}O_{10}\bullet$, are not detected in Beijing. This is possibly caused by both low monoterpene abundance (Cheng et al., 2018) and high NO_x concentration in Beijing (11.06 ppbv; Fig. S10), which lead to a low production rate and high loss rate of RO_2 radicals. Third, most MT OOMs in urban Beijing possess five or six effective oxygen atoms, whereas in the forest environment a large fraction of them can hold 7 to 10 effective oxygen atoms (Fig. 8b). This again suggests that high NO_x in Beijing effectively inhibits the oxygen addition processes (Zhao et al., 2018; Orlando and Tyndall, 2012). Additionally, high NO_x in Beijing also leads to high nitrogen content (Fig. 8c) by promoting the termination reaction between RO_2 and NO_x (Orlando and Tyndall, 2012) and facilitating the formation of NO_3 radical (H. Wang et al., 2018), which further leads to the formation of nitrate MT OOMs (Boyd et al., 2015; Nah et al., 2016).

3.2.2 Characteristics of anthropogenic OOMs

Although the oxidation pathways and product composition of a few aromatic VOCs have been studied previously, the reported products are of much less diversity compared to the complex real atmosphere. Therefore, we rely on the workflow (see Sect. 2.2 and Nie et al., 2022) to find possible aro-

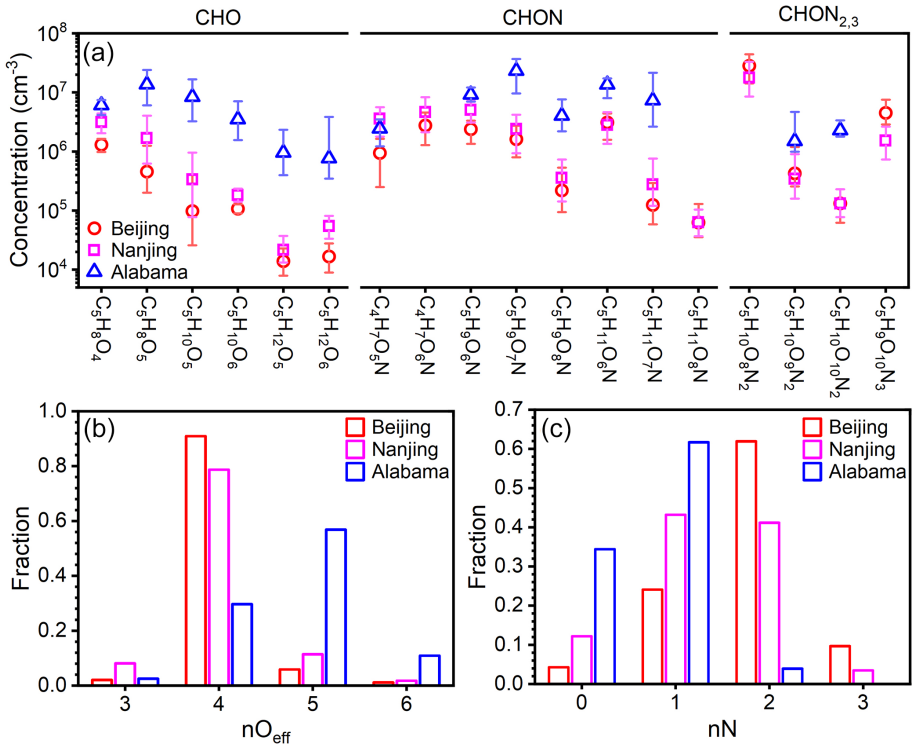

Figure 6. **(a)** Concentration comparison of specific fingerprint IP OOM molecules between our study and previously reported ones (Krechmer et al., 2015; Massoli et al., 2018; Liu et al., 2021). The markers are median concentration values, and the upper and lower bounds of the error bars denote 25th and 75th percentiles, respectively. The distribution of the **(b)** effective oxygen number, nO_{eff}, and **(c)** nitrogen number, nN, of IP OOMs is plotted in panel **(a)**.

matic OOMs in our measurement. Among the deduced aromatic OOMs, almost all C6–C9 CHO and C6 CHON compounds have been detected in previous benzene, toluene, xylene, ethylbenzene, and mesitylene experiments (Molteni et al., 2018; Garmash et al., 2020; see detail in Table S9), which demonstrates the reliability of our workflow.

As shown in Fig. 9a to d, predominant aromatic species in different seasons possess a high similarity, and they could be classified into $C_{6–9}H_{8–14}O_4$, $C_{6–8}H_{8–12}O_5$, $C_{7,8}H_{8,10}O_5$, $C_{6–10}H_{7–15}O_6N$, $C_{7–9}H_{9–13}O_7N$, $C_{8–10}H_{11–15}O_8N$, and $C_{8,9}H_{12–14}O_{10}N_2$ categories, among which a prominent CH_2 spacing is seen. Such patterns are most likely due to the co-existence of homologous precursor VOCs, although fragmentation processes during the oxidation could also play a role (Pan and Wang, 2014; Zaytsev et al., 2019; Xu et al., 2020). Besides, the distribution of CHON aromatic OOMs in winter and autumn are very similar, with $C_8H_{11}O_6N$ being the highest; in comparison, the overall distribution moves to higher oxygen content in summer, e.g., $C_8H_{11}O_7N$ becomes the largest one. This suggests that the enhancement of radiation, which leads to strong photochemistry and high temperature, and the reduction of NO_x in summer benefit the formation of highly oxygenated organic molecules (Garmash et al., 2020; Orlando and Tyndall, 2012). There are also fingerprint molecules for different seasons, such as $C_{10}H_8O_6$ in spring, $C_9H_{10}O_{11}N_2$ in summer, and $C_{10}H_6O_4$ in summer and autumn. Due to the complexity of real atmosphere, the reason for their seasonal variation is unclear, and further analysis is warranted. In terms of nitrogen content, aromatic OOMs contain large fraction of CHO (42 %–52 %) and CHON (39 %–51 %) species. The contribution of $CHON_2$ OOMs reaches the highest in summer, which again indicates that the involvement of NO_x is enhanced under the influence of elevated UVB and temperature. The carbon distribution among seasons are very similar (Fig. S13), where C4 to C9 aromatic OOMs, probably derived from monocyclic aromatic hydrocarbons, make up 68 %–76 % and other $C \geq 10$ ones, of which 59 %–68 % are likely the oxidation products from PAHs (DBE≥5; Table S10), take up 24 %–32 %. This implies that the relative abundance of emitted aromatic precursors with different carbon atoms is quite stable during the year.

Major aliphatic OOM molecules in different seasons are highly similar, and they possess more evident homologous patterns than aromatic OOMs (Fig. 9e to h and Table S11). The dominant species of aliphatic OOMs are $C_{6–9}H_{10–16}O_4$, $C_{6–10}H_{11–19}O_6N$, $C_{5–10}H_{7–17}O_6N$, $C_{5–10}H_{8–18}O_8N_2$, and $C_{6–9}H_{12–18}O_7N_2$, and some less oxygenated compounds, e.g., $C_{6–8}H_{11–15}O_5N$, also have considerable contributions in winter and autumn. For nitrogen content, CHO aliphatic

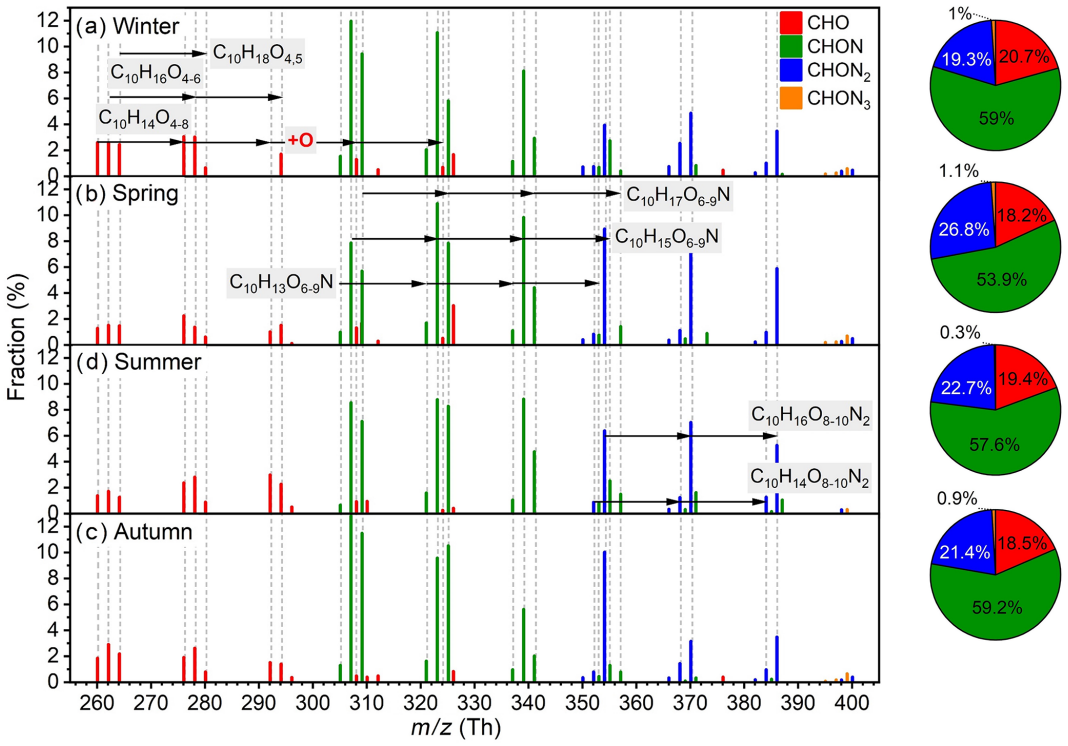

Figure 7. Fractional profiles of each MT OOM molecule in **(a)** winter, **(b)** spring, **(c)** summer, and **(d)** autumn. The mass-to-charge ratio (m/z) denotes OOM clustered with NO_3^- or as deprotonated ones. The fraction of each compound is calculated as the ratio of its concentration to the total concentration of MT OOMs. The red, green, blue, and orange bars are for CHO, CHON, $CHON_2$, and $CHON_3$ OOMs, respectively.

OOMs only take a small fraction of 8 %–11 %, implying that the NO_x termination may dominate the formation of aliphatic closed-shell molecules. Meanwhile, this CHO OOM fraction of aliphatic OOMs is much smaller than that of aromatic OOMs (42 %–52 %), suggesting that the branching ratio of the aliphatic RO_2–NO_x reaction forming $CHON_x$ species is higher than that of the aromatic one. Besides, unlike aromatic OOMs, aliphatic $CHON_2$ OOMs have a bigger contribution in winter than in the other three seasons. This is because a major sequence of $CHON_2$ OOMs, $C_{6–14}H_{12–28}O_7N_2$, is found to coincide with $PM_{2.5}$ (Fig. S14), which is frequently high in winter. In winter in Beijing, the regional transportation of air masses from the southern and southeastern areas is a large source of $PM_{2.5}$ (Wang et al., 2015; Chen et al., 2021, 2022; Tan et al., 2022); therefore, the good correlation between $CHON_2$ species and $PM_{2.5}$ suggests that those compounds might also have regional sources. Table S12 shows that $C_{6–10}H_{12–20}O_7N_2$ are relatively volatile and are classified as semi-volatile organic compounds; thus, they could originate from long-distance transport. It is very likely that they are equilibrated in larger gas-phase concentrations as SOA also increases with the elevation of $PM_{2.5}$ (Fig. S15). For $C_{11–14}H_{22–28}O_7N_2$, they are less volatile and lie in the range of LVOCs; hence, they can hardly be transported and are more likely produced during the air mass transportation. Those pollution-related OOMs take the largest (14 %) and smallest (2 %) fraction in winter and summer, respectively (Table S11). In terms of carbon distribution, there is not too much difference among seasons because the relatively short C4 to C9 aliphatic OOMs make up 83 %–90 % and the longer ones take up 10 %–17 % (Fig. S13).

Up until now, field measurements of anthropogenic OOMs have been rare (Nie et al., 2022; Liu et al., 2021). In general, the concentrations of aromatic and aliphatic OOMs in Beijing are comparable with those in other Chinese megacities (Table S13), and fingerprint aromatic and aliphatic OOM molecules in Beijing and Nanjing are also identical (Table S14). This suggests that the OOM production, including both the precursor emissions and oxidation mechanisms, may share high similarities in megacities. Yet, a more systematic comparison can only be made when measurements at more locations are available in the future.

3.3 Atmospheric implication: OOM contribution to SOA through condensation

The volatility of the organic compound determines its partitioning between gas and particle phases, and thus influences its atmospheric lifetime, gas-phase concentration, and contribution to SOA. Therefore, we estimate the volatility of

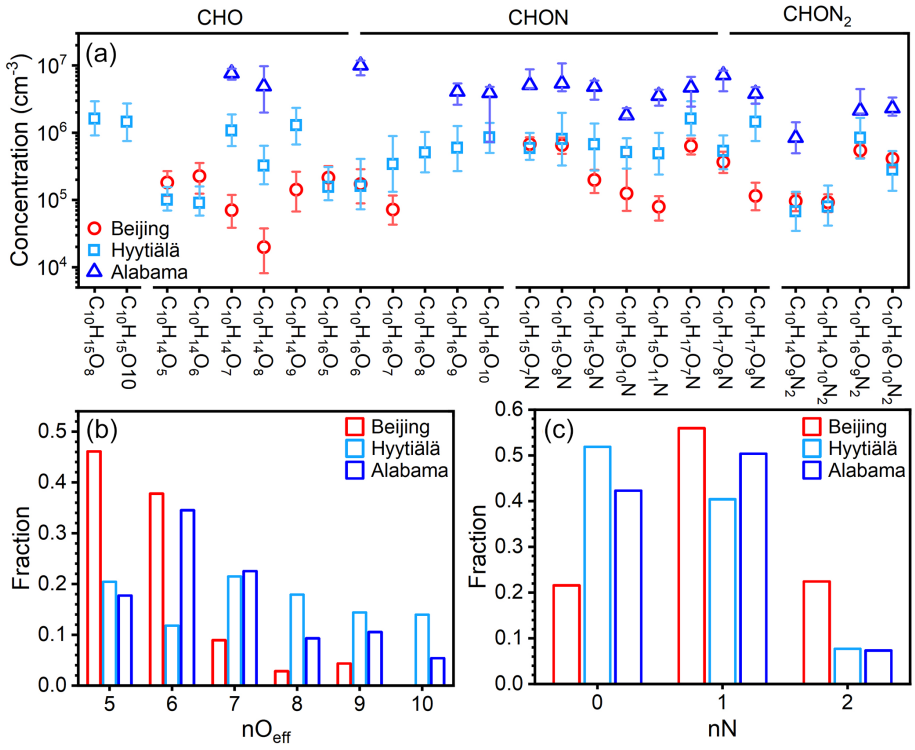

Figure 8. **(a)** Concentration comparison of specific fingerprint MT OOM molecules between our study and previously reported ones (Massoli et al., 2018; Yan et al., 2016). The markers are median concentration values, and the upper and lower bounds of the error bars denote 25th and 75th percentiles, respectively. Please note that only the summer Beijing data were plotted as the overall pattern of MT OOMs in Beijing summer and spring are very similar (Fig. 7). The distribution of the **(b)** effective oxygen number, nO_{eff}, and **(c)** nitrogen number, nN, of MT OOMs is plotted in panel **(a)**.

source-classified OOMs (the detailed method can be found in Sect. S3) and summarize the results in Fig. 10. The seasonal variations in OOMs classified as ELVOCs (extremely low volatility organic compounds), LVOCs (low volatility organic compounds) and SVOCs (semi-volatile organic compounds) follow the same trend as that of total OOMs, with the highest concentrations in summer (1.3×10^7, 4.0×10^7, and 8.4×10^7 cm^{-3} for ELVOCs, LVOCs, and SVOCs, respectively) and the lowest ones in winter (4.4×10^6, 9.4×10^6, and 5.3×10^6 cm^{-3} for ELVOCs, LVOCs, and SVOCs, respectively). Here, we focus particularly on OOMs with relatively low volatility with high potential contributing to the formation of SOA.

Due to the concentration variation in four source-classified OOMs and their temperature-dependent volatility distribution (Table S16), their fractions within different volatility ranges have distinct seasonal characteristics (Fig. 10b). Among ELVOCs, aromatic OOMs take the largest fractions, ranging from 72 % to 94 % throughout the year. For LVOCs, aromatic (34 %–51 %) and aliphatic OOMs (17 %–42 %) are the two that have the largest proportions. And MT OOMs, favored by their low volatility (Table S16; Tröstl et al., 2016; Yan et al., 2020), also take up ∼ 14 % of LVOCs in seasons other than winter. IP OOMs, however, due to their high volatility (Table S16; Krechmer et al., 2015; Xu et al., 2021), do not have an appreciable contribution to ELVOCs and LVOCs – even in summer, when the concentration is exceedingly high. Consequently, it is likely that the pure condensation of IP OOMs has a minor contribution to SOA growth, regardless of the season.

The rate of OOM condensation onto particles, referred to as condensation flux hereafter, was calculated based on the particle dynamic model proposed by Tröstl et al. (2016; see details in Sect. S5). In terms of seasonal variation (Fig. 11a), OOM condensation flux exhibits the highest level in autumn (0.64 µg m^{-3} h^{-1}), followed by summer (0.61 µg m^{-3} h^{-1}) and spring (0.41 µg m^{-3} h^{-1}) and decreases to the lowest in winter (0.30 µg m^{-3} h^{-1}). For a seasonal comparison of the SOA formation rate caused by OOM condensation, the characteristic accumulation time (AccTime), defined as SOA divided by OOM condensation flux, is calculated as an indicator (see details in Sect. S4). As shown in Fig. 11b, a characteristic time of 24 h is enough to explain the observed SOA concentration by OOM condensation in winter, and it is reduced to 7, 10, and 7 h for spring, summer, and autumn, respectively. It should be noted that this should not be interpreted as the entire SOA being formed via OOM condensation during this characteristic time but rather that OOM con-

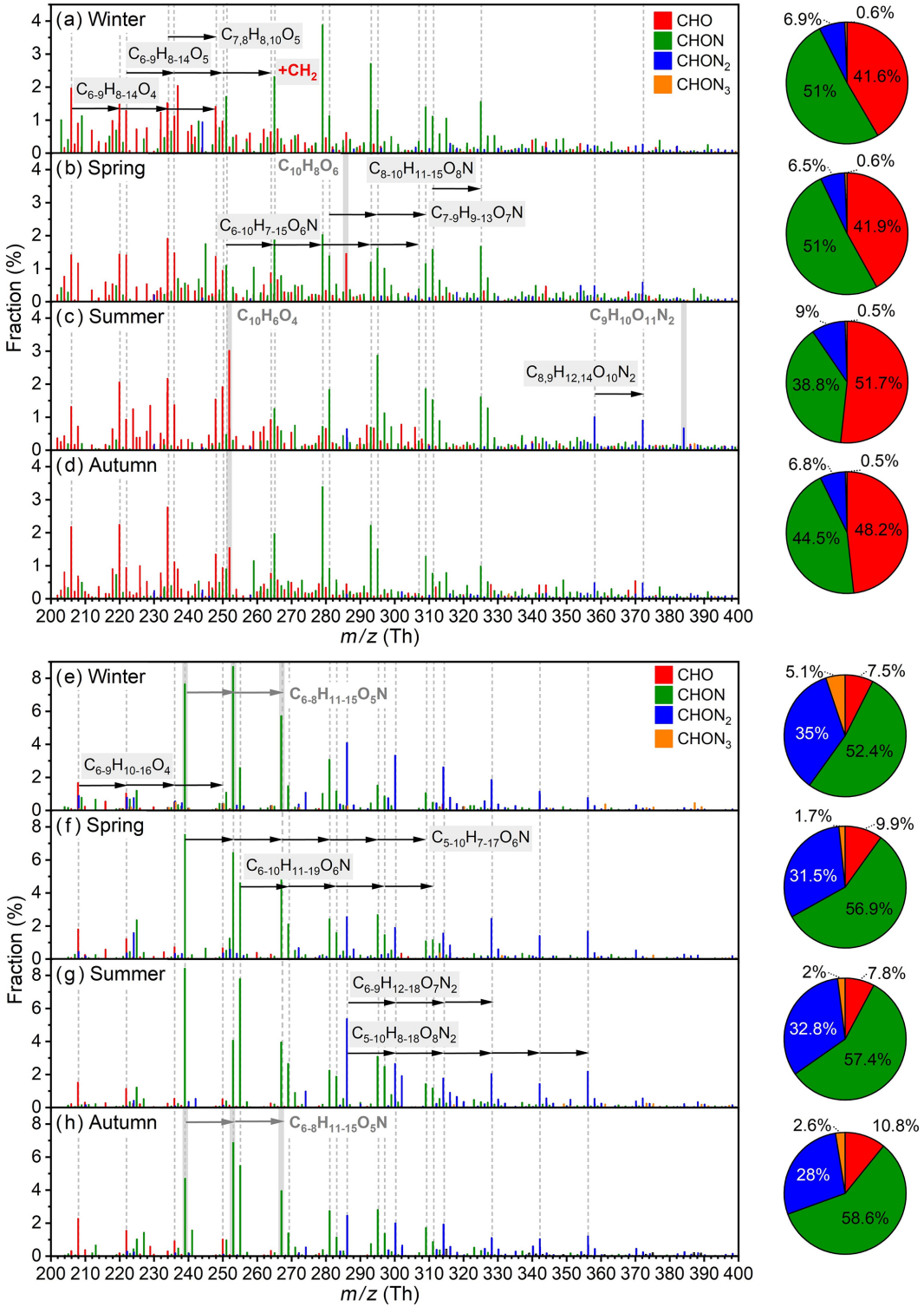

Figure 9. Fractional profiles of each aromatic OOM molecule in **(a)** winter, **(b)** spring, **(c)** summer, and **(d)** autumn and of each aliphatic OOM molecule in **(e)** winter, **(f)** spring, **(g)** summer, and **(h)** autumn. The mass-to-charge ratio (m/z) denotes OOM clustered with NO_3^- or as deprotonated ones. The fraction of each compound is calculated as the ratio of its concentration to the total concentration of aromatic OOMs **(a–d)** or aliphatic OOMs **(e–h)**. The red, green, blue, and orange bars are for CHO, CHON, $CHON_2$, and $CHON_3$ OOMs, respectively. Species marked with gray dashed lines are primary ones during the year, and species with a gray shading are special ones for specific seasons.

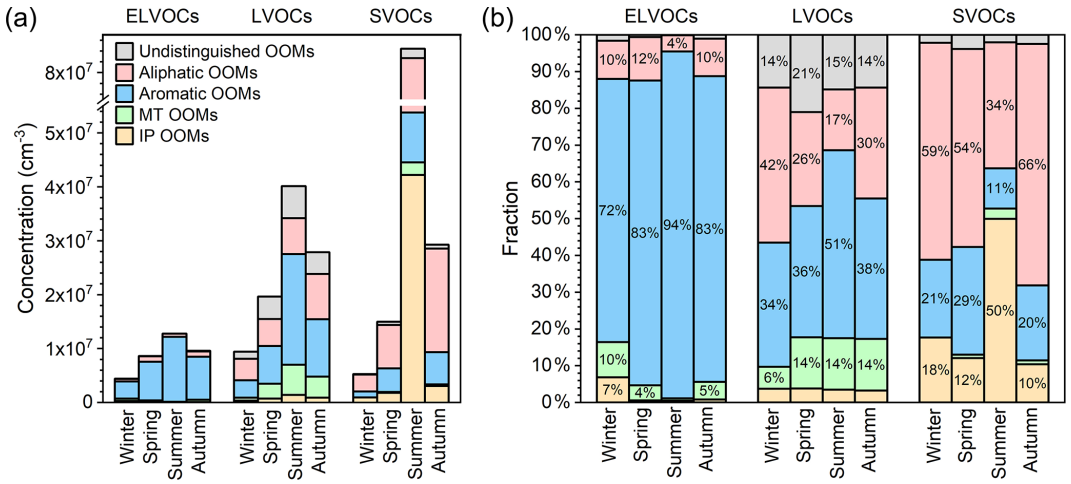

Figure 10. **(a)** Concentration and **(b)** fraction of source-classified OOMs in ELVOCs (extremely low volatile organic compounds), LVOCs (low volatile organic compounds), and SVOCs (semi-volatile organic compounds) in four seasons. Please also note that the fractions smaller than 4 % are not marked.

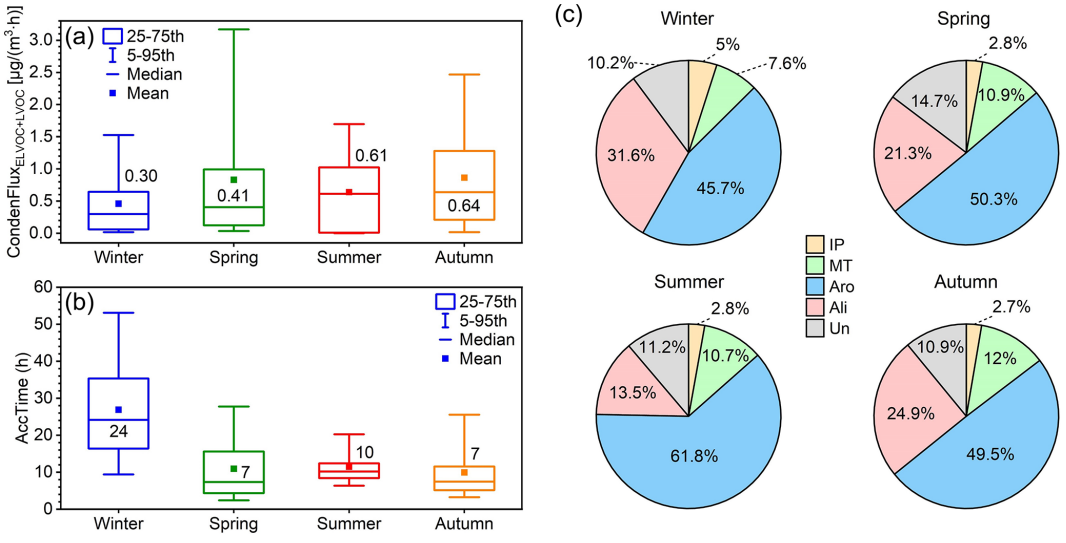

Figure 11. **(a)** Condensation flux of OOMs calculated by the particle dynamic model by Tröstl et al. (2016) in four seasons. **(b)** Characteristic accumulation time of SOA (AccTime), calculated as SOA divided by OOM condensation flux, in four seasons. This parameter is used as an indicator of the relative accumulation rate of SOA caused by OOM condensation in different seasons. The values in each box of panels **(a)** and **(b)** are the median values of corresponding parameters. **(c)** Estimated condensation flux contribution of four source-classified OOMs in four seasons. The abbreviations IP, MT, Aro, Ali, and Un stand for IP OOMs, MT OOMs, aromatic OOMs, aliphatic OOMs, and undistinguished OOMs, respectively.

densation is efficient and can have a significant contribution to SOA formation. A recent study (Nie et al., 2022) suggested that OOM condensation can account for about 40 % of the SOA formation in wintertime in Beijing. Our analysis of the seasonal variation indicates that the condensation of OOMs could have a larger contribution to SOA formation in seasons other than winter.

For OOMs from different sources, aromatic OOMs contribute the most during the year, varying from 46 % to 62 %, followed by aliphatic OOMs (14 %–32 %). In comparison, the two biogenic ones, MT OOMs (8 %–12 %) and IP OOMs (3 %–5 %), have a smaller contribution in all four seasons. This indicates that the formation of SOA through condensation in urban Beijing is dominated by anthropogenic sources, which is in line with the previously reported SOA composition (Le Breton et al., 2018; Mehra et al., 2021). Overall, our results suggest that, in order to control the formation of SOA, the emission of anthropogenic VOCs, especially aromatics, should be restricted with a high priority.

4 Summary and conclusions

A long-term measurement of OOMs based on nitrate CIMS was conducted in urban Beijing. OOMs in the mass range of 200–400 Th were systematically investigated. Total OOM concentration in Beijing shows a clear dependence on UVB and temperature, suggesting the importance of photooxidation and temperature on OOM formation. In comparison to other atmospheric sites, total OOM concentration in Beijing (2.3×10^7–1.6×10^8 cm^{-3}) is generally comparable to urban and suburban areas and is clearly lower than those measured in forested areas. In the case of composition, most OOMs have 5 to 10 carbon atoms, 3 to 7 effective oxygen atoms, 0 to 2 nitrogen atoms, and 0 to 6 DBE values. The seasonal variation in the average effective oxygen atom follows the same trend as the overall atmospheric oxidation capacity, which is the highest in summer and the lowest in winter and autumn. While, for nitrogen and DBE distribution, there is not too much difference among seasons disregarding isoprene OOMs, indicating that the dominant formation pathways of each source-classified OOMs stay constant during the year.

With a revised workflow, we further separate OOMs into isoprene, monoterpene, aromatic, and aliphatic OOMs. For relative abundance, aromatic (29 %–41 %) and aliphatic OOMs (26 %–41 %) are major contributors throughout the year, suggesting that OOMs in the urban atmospheric environment are controlled by anthropogenic activities. In addition, isoprene OOMs play an important role in summer, and their fraction reaches to 33 %, indicating that biogenic sources are also large contributors to total OOMs in warmer seasons. The concentrations of isoprene OOMs (0.2–5.3×10^7 cm^{-3}) and monoterpene OOMs (1.1–8.4×10^6 cm^{-3}) are smaller than those in forested areas, and they exhibit higher nitrogen and lower oxygen content compared with other cleaner sites. One recent study (Nie et al., 2022) reported that the composition of wintertime OOMs among four Chinese megacities, including Beijing, were similar. Our study further demonstrates that the composition of summertime OOMs between Beijing and Nanjing also have a strong resemblance. Consequently, the seasonal characteristics of Beijing OOMs in this study could be representative of OOMs in other Chinese metropolises.

In terms of volatility, monoterpene OOMs are the most condensable, isoprene OOMs are the most volatile, and aromatic OOMs are more condensable than aliphatic ones. Based on the volatility and concentration characteristics of the four source-classified OOMs, an aerosol growth model was utilized to calculate their contribution to SOA growth. Results show that the condensation flux of total OOMs (0.30–0.64 µg m^{-3} h^{-1}) are high enough to produce a considerable amount of SOA within a day, and that aromatic (46 %–62 %) and aliphatic (14 %–32 %) OOMs are found to be dominant contributors regardless of the season. This suggests that the formation of SOA in urban cities is likely driven by OOMs from anthropogenic sources and highlights the importance of reducing anthropogenic emissions, especially aromatics, for pollution mitigation.

Data availability. Data and materials are available upon request from the first author (sevenleaves1993@126.com) and corresponding author (chaoyan@nju.edu.cn).

Supplement. The supplement related to this article is available online at: https://doi.org/10.5194/acp-22-10077-2022-supplement.

Author contributions. CY and YG designed the study and wrote the paper. YG, YL, FZ, YiZhang, YZho, CL, XF, ZL, ZF, YuZhang, PZ, and LT conducted the measurement and collected the data. CY, WN, ZW, DH, XQ, YL, YG, PZ, and LT built the workflow and contributed to the aerosol dynamic model. JJ and VMK modified the paper. And all co-authors have read and commented on the paper.

Competing interests. The contact author has declared that none of the authors has any competing interests.

Disclaimer. Publisher's note: Copernicus Publications remains neutral with regard to jurisdictional claims in published maps and institutional affiliations.

Acknowledgements. Heikki Junninen is acknowledged, for providing the tofTool package used for processing LTOF-CIMS data.

Financial support. This work has been supported by the National Natural Science Foundation of China (NSFC) project (grant nos. 41875175, 42075101, and 22188102) and Samsung $PM_{2.5}$ SRP. Kaspar R. Daellenbach acknowledges support by the Swiss National Science Foundation Ambizione (grant no. PZPGP2_201992).

Open-access funding was provided by the Helsinki University Library.

Review statement. This paper was edited by Arthur Chan and reviewed by two anonymous referees.

References

Aalto, P., Hämeri, K., Becker, E., Weber, R., Salm, J., Mäkelä, J. M., Hoell, C., O'dowd, C. D., Hansson, H.-C., Väkevä, M., Koponen, I. K., Buzorius, G., and Kulmala, M.: Physical characterization of aerosol particles during nucleation events, Tellus B, 53, 344–358, https://doi.org/10.3402/tellusb.v53i4.17127, 2001.

Berndt, T., Richters, S., Jokinen, T., Hyttinen, N., Kurtén, T., Otkjær, R. V., Kjaergaard, H. G., Stratmann, F., Herrmann, H., Sipilä, M., Kulmala, M., and Ehn, M.: Hydroxyl radical-induced formation of highly oxidized organic compounds, Nat. Commun., 7, 13677, https://doi.org/10.1038/ncomms13677, 2016.

Berndt, T., Mentler, B., Scholz, W., Fischer, L., Herrmann, H., Kulmala, M., and Hansel, A.: Accretion Product Formation from Ozonolysis and OH Radical Reaction of α-Pinene: Mechanistic Insight and the Influence of Isoprene and Ethylene, Environ. Sci. Technol., 52, 11069–11077, https://doi.org/10.1021/acs.est.8b02210, 2018.

Bianchi, F., Tröstl, J., Junninen, H., Frege, C., Henne, S., Hoyle, C. R., Molteni, U., Herrmann, E., Adamov, A., Bukowiecki, N., Chen, X., Duplissy, J., Gysel, M., Hutterli, M., Kangasluoma, J., Kontkanen, J., Kürten, A., Manninen, H. E., Münch, S., Peräkylä, O., Petäjä, T., Rondo, L., Williamson, C., Weingartner, E., Curtius, J., Worsnop, D. R., Kulmala, M., Dommen, J., and Baltensperger, U.: New particle formation in the free troposphere: A question of chemistry and timing, Science, 352, 1109–1112, https://doi.org/10.1126/science.aad5456, 2016.

Bianchi, F., Garmash, O., He, X., Yan, C., Iyer, S., Rosendahl, I., Xu, Z., Rissanen, M. P., Riva, M., Taipale, R., Sarnela, N., Petäjä, T., Worsnop, D. R., Kulmala, M., Ehn, M., and Junninen, H.: The role of highly oxygenated molecules (HOMs) in determining the composition of ambient ions in the boreal forest, Atmos. Chem. Phys., 17, 13819–13831, https://doi.org/10.5194/acp-17-13819-2017, 2017.

Bianchi, F., Kurten, T., Riva, M., Mohr, C., Rissanen, M. P., Roldin, P., Berndt, T., Crounse, J. D., Wennberg, P. O., Mentel, T. F., Wildt, J., Junninen, H., Jokinen, T., Kulmala, M., Worsnop, D. R., Thornton, J. A., Donahue, N., Kjaergaard, H. G., and Ehn, M.: Highly Oxygenated Organic Molecules (HOM) from Gas-Phase Autoxidation Involving Peroxy Radicals: A Key Contributor to Atmospheric Aerosol, Chem. Rev., 119, 3472–3509, https://doi.org/10.1021/acs.chemrev.8b00395, 2019.

Boyd, C. M., Sanchez, J., Xu, L., Eugene, A. J., Nah, T., Tuet, W. Y., Guzman, M. I., and Ng, N. L.: Secondary organic aerosol formation from the β-pinene + NO_3 system: effect of humidity and peroxy radical fate, Atmos. Chem. Phys., 15, 7497–7522, https://doi.org/10.5194/acp-15-7497-2015, 2015.

Brean, J., Harrison, R. M., Shi, Z., Beddows, D. C. S., Acton, W. J. F., Hewitt, C. N., Squires, F. A., and Lee, J.: Observations of highly oxidized molecules and particle nucleation in the atmosphere of Beijing, Atmos. Chem. Phys., 19, 14933–14947, https://doi.org/10.5194/acp-19-14933-2019, 2019.

Caudillo, L., Rörup, B., Heinritzi, M., Marie, G., Simon, M., Wagner, A. C., Müller, T., Granzin, M., Amorim, A., Ataei, F., Baalbaki, R., Bertozzi, B., Brasseur, Z., Chiu, R., Chu, B., Dada, L., Duplissy, J., Finkenzeller, H., Gonzalez Carracedo, L., He, X.-C., Hofbauer, V., Kong, W., Lamkaddam, H., Lee, C. P., Lopez, B., Mahfouz, N. G. A., Makhmutov, V., Manninen, H. E., Marten, R., Massabò, D., Mauldin, R. L., Mentler, B., Molteni, U., Onnela, A., Pfeifer, J., Philippov, M., Piedehierro, A. A., Schervish, M., Scholz, W., Schulze, B., Shen, J., Stolzenburg, D., Stozhkov, Y., Surdu, M., Tauber, C., Tham, Y. J., Tian, P., Tomé, A., Vogt, S., Wang, M., Wang, D. S., Weber, S. K., Welti, A., Yonghong, W., Yusheng, W., Zauner-Wieczorek, M., Baltensperger, U., El Haddad, I., Flagan, R. C., Hansel, A., Höhler, K., Kirkby, J., Kulmala, M., Lehtipalo, K., Möhler, O., Saathoff, H., Volkamer, R., Winkler, P. M., Donahue, N. M., Kürten, A., and Curtius, J.: Chemical composition of nanoparticles from α-pinene nucleation and the influence of isoprene and relative humidity at low temperature, Atmos. Chem. Phys., 21, 17099–17114, https://doi.org/10.5194/acp-21-17099-2021, 2021.

Chen, D., Xia, L., Guo, X., Lang, J., Zhou, Y., Wei, L., and Fu, X.: Impact of inter-annual meteorological variation from 2001 to 2015 on the contribution of regional transport to $PM_{2.5}$ in Beijing, China, Atmos. Environ., 260, 118545, https://doi.org/10.1016/j.atmosenv.2021.118545, 2021.

Chen, D., Jin, X., Fu, X., Xia, L., Guo, X., Lang, J., Zhou, Y., and Wei, W.: Impact of Inter-Annual Variation in Meteorology from 2010 to 2019 on the Inter-City Transport of $PM_{2.5}$ in the Beijing–Tianjin–Hebei Region, Sustainability, 14, 6210, https://doi.org/10.3390/su14106210, 2022.

Cheng, X., Li, H., Zhang, Y., Li, Y., Zhang, W., Wang, X., Bi, F., Zhang, H., Gao, J., Chai, F., Lun, X., Chen, Y., Gao, J., and Lv, J.: Atmospheric isoprene and monoterpenes in a typical urban area of Beijing: Pollution characterization, chemical reactivity and source identification, J. Environ. Sci., 71, 150–167, https://doi.org/10.1016/j.jes.2017.12.017, 2018.

Dada, L., Paasonen, P., Nieminen, T., Buenrostro Mazon, S., Kontkanen, J., Peräkylä, O., Lehtipalo, K., Hussein, T., Petäjä, T., Kerminen, V. M., Bäck, J., and Kulmala, M.: Long-term analysis of clear-sky new particle formation events and nonevents in Hyytiälä, Atmos. Chem. Phys., 17, 6227–6241, https://doi.org/10.5194/acp-17-6227-2017, 2017.

Donahue, N. M., Ortega, I. K., Chuang, W., Riipinen, I., Riccobono, F., Schobesberger, S., Dommen, J., Baltensperger, U., Kulmala, M., Worsnop, D. R., and Vehkamaki, H.: How do organic vapors contribute to new-particle formation?, Faraday Discuss., 165, 91–104, https://doi.org/10.1039/C3FD00046J, 2013.

Drewnick, F., Hings, S. S., DeCarlo, P., Jayne, J. T., Gonin, M., Fuhrer, K., Weimer, S., Jimenez, J. L., Demerjian, K. L., Borrmann, S., and Worsnop, D. R.: A New Time-of-Flight Aerosol Mass Spectrometer (TOF-AMS) – Instrument Description and First Field Deployment, Aerosol Sci. Tech., 39, 637–658, https://doi.org/10.1080/02786820500182040, 2005.

Ehn, M., Junninen, H., Petäjä, T., Kurtén, T., Kerminen, V. M., Schobesberger, S., Manninen, H. E., Ortega, I. K., Vehkamäki, H., Kulmala, M., and Worsnop, D. R.: Composition and temporal behavior of ambient ions in the boreal forest, Atmos. Chem. Phys., 10, 8513–8530, https://doi.org/10.5194/acp-10-8513-2010, 2010.

Ehn, M., Kleist, E., Junninen, H., Petäjä, T., Lönn, G., Schobesberger, S., Dal Maso, M., Trimborn, A., Kulmala, M., Worsnop, D. R., Wahner, A., Wildt, J., and Mentel, T. F.: Gas phase formation of extremely oxidized pinene reaction products in chamber and ambient air, Atmos. Chem. Phys., 12, 5113–5127, https://doi.org/10.5194/acp-12-5113-2012, 2012.

Ehn, M., Thornton, J. A., Kleist, E., Sipilä, M., Junninen, H., Pullinen, I., Springer, M., Rubach, F., Tillmann, R., Lee, B.,

Lopez-Hilfiker, F., Andres, S., Acir, I.-H., Rissanen, M., Jokinen, T., Schobesberger, S., Kangasluoma, J., Kontkanen, J., Nieminen, T., Kurtén, T., Nielsen, L. B., Jørgensen, S., Kjaergaard, H. G., Canagaratna, M., Maso, M. D., Berndt, T., Petäjä, T., Wahner, A., Kerminen, V.-M., Kulmala, M., Worsnop, D. R., Wildt, J., and Mentel, T. F.: A large source of low-volatility secondary organic aerosol, Nature, 506, 476–479, https://doi.org/10.1038/nature13032, 2014.

Garmash, O., Rissanen, M. P., Pullinen, I., Schmitt, S., Kausiala, O., Tillmann, R., Zhao, D., Percival, C., Bannan, T. J., Priestley, M., Hallquist, A. M., Kleist, E., Kiendler-Scharr, A., Hallquist, M., Berndt, T., McFiggans, G., Wildt, J., Mentel, T., and Ehn, M.: Multi-generation OH oxidation as a source for highly oxygenated organic molecules from aromatics, Atmos. Chem. Phys., 20, 515–537, https://doi.org/10.5194/acp-20-515-2020, 2020.

Gordon, H., Kirkby, J., Baltensperger, U., Bianchi, F., Breitenlechner, M., Curtius, J., Dias, A., Dommen, J., Donahue, N. M., Dunne, E. M., Duplissy, J., Ehrhart, S., Flagan, R. C., Frege, C., Fuchs, C., Hansel, A., Hoyle, C. R., Kulmala, M., Kürten, A., Lehtipalo, K., Makhmutov, V., Molteni, U., Rissanen, M. P., Stozkhov, Y., Tröstl, J., Tsagkogeorgas, G., Wagner, R., Williamson, C., Wimmer, D., Winkler, P. M., Yan, C., and Carslaw, K. S.: Causes and importance of new particle formation in the present-day and preindustrial atmospheres, J. Geophys. Res.-Atmos., 122, 8739–8760, https://doi.org/10.1002/2017JD026844, 2017.

Guo, Y., Yan, C., Li, C., Ma, W., Feng, Z., Zhou, Y., Lin, Z., Dada, L., Stolzenburg, D., Yin, R., Kontkanen, J., Daellenbach, K. R., Kangasluoma, J., Yao, L., Chu, B., Wang, Y., Cai, R., Bianchi, F., Liu, Y., and Kulmala, M.: Formation of nighttime sulfuric acid from the ozonolysis of alkenes in Beijing, Atmos. Chem. Phys., 21, 5499–5511, https://doi.org/10.5194/acp-21-5499-2021, 2021.

Hallquist, M., Wenger, J. C., Baltensperger, U., Rudich, Y., Simpson, D., Claeys, M., Dommen, J., Donahue, N. M., George, C., Goldstein, A. H., Hamilton, J. F., Herrmann, H., Hoffmann, T., Iinuma, Y., Jang, M., Jenkin, M. E., Jimenez, J. L., Kiendler-Scharr, A., Maenhaut, W., McFiggans, G., Mentel, T. F., Monod, A., Prevot, A. S. H., Seinfeld, J. H., Surratt, J. D., Szmigielski, R., and Wildt, J.: The formation, properties and impact of secondary organic aerosol: current and emerging issues, Atmos. Chem. Phys., 9, 5155–5236, https://doi.org/10.5194/acp-9-5155-2009, 2009.

Heinritzi, M., Simon, M., Steiner, G., Wagner, A. C., Kürten, A., Hansel, A., and Curtius, J.: Characterization of the mass-dependent transmission efficiency of a CIMS, Atmos. Meas. Tech., 9, 1449–1460, https://doi.org/10.5194/amt-9-1449-2016, 2016.

Heinritzi, M., Dada, L., Simon, M., Stolzenburg, D., Wagner, A. C., Fischer, L., Ahonen, L. R., Amanatidis, S., Baalbaki, R., Baccarini, A., Bauer, P. S., Baumgartner, B., Bianchi, F., Brilke, S., Chen, D., Chiu, R., Dias, A., Dommen, J., Duplissy, J., Finkenzeller, H., Frege, C., Fuchs, C., Garmash, O., Gordon, H., Granzin, M., El Haddad, I., He, X., Helm, J., Hofbauer, V., Hoyle, C. R., Kangasluoma, J., Keber, T., Kim, C., Kürten, A., Lamkaddam, H., Laurila, T. M., Lampilahti, J., Lee, C. P., Lehtipalo, K., Leiminger, M., Mai, H., Makhmutov, V., Manninen, H. E., Marten, R., Mathot, S., Mauldin, R. L., Mentler, B., Molteni, U., Müller, T., Nie, W., Nieminen, T., Onnela, A., Partoll, E., Passananti, M., Petäjä, T., Pfeifer, J., Pospisilova, V., Quéléver, L. L. J., Rissanen, M. P., Rose, C., Schobesberger, S., Scholz, W., Scholze, K., Sipilä, M., Steiner, G., Stozhkov, Y., Tauber, C., Tham, Y. J., Vazquez-Pufleau, M., Virtanen, A., Vogel, A. L., Volkamer, R., Wagner, R., Wang, M., Weitz, L., Wimmer, D., Xiao, M., Yan, C., Ye, P., Zha, Q., Zhou, X., Amorim, A., Baltensperger, U., Hansel, A., Kulmala, M., Tomé, A., Winkler, P. M., Worsnop, D. R., Donahue, N. M., Kirkby, J., and Curtius, J.: Molecular understanding of the suppression of new-particle formation by isoprene, Atmos. Chem. Phys., 20, 11809–11821, https://doi.org/10.5194/acp-20-11809-2020, 2020.

Huang, W., Li, H., Sarnela, N., Heikkinen, L., Tham, Y. J., Mikkilä, J., Thomas, S. J., Donahue, N. M., Kulmala, M., and Bianchi, F.: Measurement report: Molecular composition and volatility of gaseous organic compounds in a boreal forest – from volatile organic compounds to highly oxygenated organic molecules, Atmos. Chem. Phys., 21, 8961–8977, https://doi.org/10.5194/acp-21-8961-2021, 2021.

Hyttinen, N., Kupiainen-Määttä, O., Rissanen, M. P., Muuronen, M., Ehn, M., and Kurtén, T.: Modeling the Charging of Highly Oxidized Cyclohexene Ozonolysis Products Using Nitrate-Based Chemical Ionization, J. Phys. Chem. A, 119, 6339–6345, https://doi.org/10.1021/acs.jpca.5b01818, 2015.

Hyttinen, N., Otkjær, R. V., Iyer, S., Kjaergaard, H. G., Rissanen, M. P., Wennberg, P. O., and Kurtén, T.: Computational Comparison of Different Reagent Ions in the Chemical Ionization of Oxidized Multifunctional Compounds, J. Phys. Chem. A, 122, 269–279, https://doi.org/10.1021/acs.jpca.7b10015, 2018.

Jayne, J. T., Leard, D. C., Zhang, X., Davidovits, P., Smith, K. A., Kolb, C. E., and Worsnop, D. R.: Development of an Aerosol Mass Spectrometer for Size and Composition Analysis of Submicron Particles, Aerosol Sci. Tech., 33, 49–70, https://doi.org/10.1080/027868200410840, 2000.

Jimenez, J. L., Canagaratna, M. R., Donahue, N. M., Prevot, A. S. H., Zhang, Q., Kroll, J. H., DeCarlo, P. F., Allan, J. D., Coe, H., Ng, N. L., Aiken, A. C., Docherty, K. S., Ulbrich, I. M., Grieshop, A. P., Robinson, A. L., Duplissy, J., Smith, J. D., Wilson, K. R., Lanz, V. A., Hueglin, C., Sun, Y. L., Tian, J., Laaksonen, A., Raatikainen, T., Rautiainen, J., Vaattovaara, P., Ehn, M., Kulmala, M., Tomlinson, J. M., Collins, D. R., Cubison, M. J., Dunlea, J., Huffman, J. A., Onasch, T. B., Alfarra, M. R., Williams, P. I., Bower, K., Kondo, Y., Schneider, J., Drewnick, F., Borrmann, S., Weimer, S., Demerjian, K., Salcedo, D., Cottrell, L., Griffin, R., Takami, A., Miyoshi, T., Hatakeyama, S., Shimono, A., Sun, J. Y., Zhang, Y. M., Dzepina, K., Kimmel, J. R., Sueper, D., Jayne, J. T., Herndon, S. C., Trimborn, A. M., Williams, L. R., Wood, E. C., Middlebrook, A. M., Kolb, C. E., Baltensperger, U., and Worsnop, D. R.: Evolution of Organic Aerosols in the Atmosphere, Science, 326, 1525, https://doi.org/10.1126/science.1180353, 2009.

Jokinen, T., Sipilä, M., Junninen, H., Ehn, M., Lönn, G., Hakala, J., Petäjä, T., Mauldin Iii, R. L., Kulmala, M., and Worsnop, D. R.: Atmospheric sulphuric acid and neutral cluster measurements using CI-APi-TOF, Atmos. Chem. Phys., 12, 4117–4125, https://doi.org/10.5194/acp-12-4117-2012, 2012.

Jokinen, T., Sipilä, M., Richters, S., Kerminen, V.-M., Paasonen, P., Stratmann, F., Worsnop, D., Kulmala, M., Ehn, M., Herrmann, H., and Berndt, T.: Rapid Autoxidation Forms Highly Oxidized

RO_2 Radicals in the Atmosphere, Angew. Chem. Int. Edn., 53, 14596–14600, https://doi.org/10.1002/anie.201408566, 2014.

Junninen, H., Ehn, M., Petäjä, T., Luosujärvi, L., Kotiaho, T., Kostiainen, R., Rohner, U., Gonin, M., Fuhrer, K., Kulmala, M., and Worsnop, D. R.: A high-resolution mass spectrometer to measure atmospheric ion composition, Atmos. Meas. Tech., 3, 1039–1053, https://doi.org/10.5194/amt-3-1039-2010, 2010.

Kirkby, J., Duplissy, J., Sengupta, K., Frege, C., Gordon, H., Williamson, C., Heinritzi, M., Simon, M., Yan, C., Almeida, J., Tröstl, J., Nieminen, T., Ortega, I. K., Wagner, R., Adamov, A., Amorim, A., Bernhammer, A.-K., Bianchi, F., Breitenlechner, M., Brilke, S., Chen, X., Craven, J., Dias, A., Ehrhart, S., Flagan, R. C., Franchin, A., Fuchs, C., Guida, R., Hakala, J., Hoyle, C. R., Jokinen, T., Junninen, H., Kangasluoma, J., Kim, J., Krapf, M., Kürten, A., Laaksonen, A., Lehtipalo, K., Makhmutov, V., Mathot, S., Molteni, U., Onnela, A., Peräkylä, O., Piel, F., Petäjä, T., Praplan, A. P., Pringle, K., Rap, A., Richards, N. A. D., Riipinen, I., Rissanen, M. P., Rondo, L., Sarnela, N., Schobesberger, S., Scott, C. E., Seinfeld, J. H., Sipilä, M., Steiner, G., Stozhkov, Y., Stratmann, F., Tomé, A., Virtanen, A., Vogel, A. L., Wagner, A. C., Wagner, P. E., Weingartner, E., Wimmer, D., Winkler, P. M., Ye, P., Zhang, X., Hansel, A., Dommen, J., Donahue, N. M., Worsnop, D. R., Baltensperger, U., Kulmala, M., Carslaw, K. S., and Curtius, J.: Ion-induced nucleation of pure biogenic particles, Nature, 533, 521–526, https://doi.org/10.1038/nature17953, 2016.

Krechmer, J. E., Coggon, M. M., Massoli, P., Nguyen, T. B., Crounse, J. D., Hu, W., Day, D. A., Tyndall, G. S., Henze, D. K., Rivera-Rios, J. C., Nowak, J. B., Kimmel, J. R., Mauldin, R. L., Stark, H., Jayne, J. T., Sipilä, M., Junninen, H., St. Clair, J. M., Zhang, X., Feiner, P. A., Zhang, L., Miller, D. O., Brune, W. H., Keutsch, F. N., Wennberg, P. O., Seinfeld, J. H., Worsnop, D. R., Jimenez, J. L., and Canagaratna, M. R.: Formation of Low Volatility Organic Compounds and Secondary Organic Aerosol from Isoprene Hydroxyhydroperoxide Low-NO Oxidation, Environ. Sci. Technol., 49, 10330–10339, https://doi.org/10.1021/acs.est.5b02031, 2015.

Kulmala, M., Kontkanen, J., Junninen, H., Lehtipalo, K., Manninen, H. E., Nieminen, T., Petäjä, T., Sipilä, M., Schobesberger, S., Rantala, P., Franchin, A., Jokinen, T., Järvinen, E., Äijälä, M., Kangasluoma, J., Hakala, J., Aalto, P. P., Paasonen, P., Mikkilä, J., Vanhanen, J., Aalto, J., Hakola, H., Makkonen, U., Ruuskanen, T., Mauldin, R. L., 3rd, Duplissy, J., Vehkamäki, H., Bäck, J., Kortelainen, A., Riipinen, I., Kurtén, T., Johnston, M. V., Smith, J. N., Ehn, M., Mentel, T. F., Lehtinen, K. E., Laaksonen, A., Kerminen, V. M., and Worsnop, D. R.: Direct observations of atmospheric aerosol nucleation, Science, 339, 943–946, https://doi.org/10.1126/science.1227385, 2013.

Kürten, A., Bergen, A., Heinritzi, M., Leiminger, M., Lorenz, V., Piel, F., Simon, M., Sitals, R., Wagner, A. C., and Curtius, J.: Observation of new particle formation and measurement of sulfuric acid, ammonia, amines and highly oxidized organic molecules at a rural site in central Germany, Atmos. Chem. Phys., 16, 12793–12813, https://doi.org/10.5194/acp-16-12793-2016, 2016.

Le Breton, M., Wang, Y., Hallquist, Å. M., Pathak, R. K., Zheng, J., Yang, Y., Shang, D., Glasius, M., Bannan, T. J., Liu, Q., Chan, C. K., Percival, C. J., Zhu, W., Lou, S., Topping, D., Wang, Y., Yu, J., Lu, K., Guo, S., Hu, M., and Hallquist, M.: Online gas- and particle-phase measurements of organosulfates, organosulfonates and nitrooxy organosulfates in Beijing utilizing a FIGAERO ToF-CIMS, Atmos. Chem. Phys., 18, 10355–10371, https://doi.org/10.5194/acp-18-10355-2018, 2018.

Lehtipalo, K., Yan, C., Dada, L., Bianchi, F., Xiao, M., Wagner, R., Stolzenburg, D., Ahonen, L., Amorim, A., Baccarini, A., Bauer, P., Baumgartner, B., Bergen, A., Bernhammer, A.-K., Breitenlechner, M., Brilke, S., Buchholz, A., Mazon, S., Chen, D., and Worsnop, D.: Multicomponent new particle formation from sulfuric acid, ammonia, and biogenic vapors, Sci. Adv., 4, eaau5363, https://doi.org/10.1126/sciadv.aau5363, 2018.

Lelieveld, J., Evans, J. S., Fnais, M., Giannadaki, D., and Pozzer, A.: The contribution of outdoor air pollution sources to premature mortality on a global scale, Nature, 525, 367–371, https://doi.org/10.1038/nature15371, 2015.

Liu, Y., Yan, C., Feng, Z., Zheng, F., Fan, X., Zhang, Y., Li, C., Zhou, Y., Lin, Z., Guo, Y., Zhang, Y., Ma, L., Zhou, W., Liu, Z., Dada, L., Dällenbach, K., Kontkanen, J., Cai, R., Chan, T., Chu, B., Du, W., Yao, L., Wang, Y., Cai, J., Kangasluoma, J., Kokkonen, T., Kujansuu, J., Rusanen, A., Deng, C., Fu, Y., Yin, R., Li, X., Lu, Y., Liu, Y., Lian, C., Yang, D., Wang, W., Ge, M., Wang, Y., Worsnop, D. R., Junninen, H., He, H., Kerminen, V.-M., Zheng, J., Wang, L., Jiang, J., Petäjä, T., Bianchi, F., and Kulmala, M.: Continuous and comprehensive atmospheric observations in Beijing: a station to understand the complex urban atmospheric environment, Big Earth Data, 4, 295–321, https://doi.org/10.1080/20964471.2020.1798707, 2020.

Liu, Y., Nie, W., Li, Y., Ge, D., Liu, C., Xu, Z., Chen, L., Wang, T., Wang, L., Sun, P., Qi, X., Wang, J., Xu, Z., Yuan, J., Yan, C., Zhang, Y., Huang, D., Wang, Z., Donahue, N. M., Worsnop, D., Chi, X., Ehn, M., and Ding, A.: Formation of condensable organic vapors from anthropogenic and biogenic volatile organic compounds (VOCs) is strongly perturbed by NO_x in eastern China, Atmos. Chem. Phys., 21, 14789–14814, https://doi.org/10.5194/acp-21-14789-2021, 2021.

Massoli, P., Stark, H., Canagaratna, M. R., Krechmer, J. E., Xu, L., Ng, N. L., Mauldin, R. L., Yan, C., Kimmel, J., Misztal, P. K., Jimenez, J. L., Jayne, J. T., and Worsnop, D. R.: Ambient Measurements of Highly Oxidized Gas-Phase Molecules during the Southern Oxidant and Aerosol Study (SOAS) 2013, ACS Earth Space Chem., 2, 653–672, https://doi.org/10.1021/acsearthspacechem.8b00028, 2018.

Mehra, A., Canagaratna, M., Bannan, T. J., Worrall, S. D., Bacak, A., Priestley, M., Liu, D., Zhao, J., Xu, W., Sun, Y., Hamilton, J. F., Squires, F. A., Lee, J., Bryant, D. J., Hopkins, J. R., Elzein, A., Budisulistiorini, S. H., Cheng, X., Chen, Q., Wang, Y., Wang, L., Stark, H., Krechmer, J. E., Brean, J., Slater, E., Whalley, L., Heard, D., Ouyang, B., Acton, W. J. F., Hewitt, C. N., Wang, X., Fu, P., Jayne, J., Worsnop, D., Allan, J., Percival, C., and Coe, H.: Using highly time-resolved online mass spectrometry to examine biogenic and anthropogenic contributions to organic aerosol in Beijing, Faraday Discuss., 226, 382–408, https://doi.org/10.1039/D0FD00080A, 2021.

Merikanto, J., Spracklen, D. V., Mann, G. W., Pickering, S. J., and Carslaw, K. S.: Impact of nucleation on global CCN, Atmos. Chem. Phys., 9, 8601–8616, https://doi.org/10.5194/acp-9-8601-2009, 2009.

Mo, Z., Shao, M., Wang, W., Liu, Y., Wang, M., and Lu, S.: Evaluation of biogenic isoprene emissions and their contribution to ozone formation by ground-based measurements

in Beijing, China, Sci. Total Environ., 627, 1485–1494, https://doi.org/10.1016/j.scitotenv.2018.01.336, 2018.

Mohr, C., Thornton, J. A., Heitto, A., Lopez-Hilfiker, F. D., Lutz, A., Riipinen, I., Hong, J., Donahue, N. M., Hallquist, M., Petäjä, T., Kulmala, M., and Yli-Juuti, T.: Molecular identification of organic vapors driving atmospheric nanoparticle growth, Nat. Commun., 10, 4442, https://doi.org/10.1038/s41467-019-12473-2, 2019.

Molteni, U., Bianchi, F., Klein, F., El Haddad, I., Frege, C., Rossi, M. J., Dommen, J., and Baltensperger, U.: Formation of highly oxygenated organic molecules from aromatic compounds, Atmos. Chem. Phys., 18, 1909–1921, https://doi.org/10.5194/acp-18-1909-2018, 2018.

Mutzel, A., Poulain, L., Berndt, T., Iinuma, Y., Rodigast, M., Böge, O., Richters, S., Spindler, G., Sipilä, M., Jokinen, T., Kulmala, M., and Herrmann, H.: Highly Oxidized Multifunctional Organic Compounds Observed in Tropospheric Particles: A Field and Laboratory Study, Environ. Sci. Technol., 49, 7754–7761, https://doi.org/10.1021/acs.est.5b00885, 2015.

Nah, T., Sanchez, J., Boyd, C., and Ng, N.: Photochemical Aging of α-pinene and β-pinene Secondary Organic Aerosol formed from Nitrate Radical Oxidation, Environ. Sci. Technol., 50, 222–231, https://doi.org/10.1021/acs.est.5b04594, 2016.

Nie, W., Yan, C., Huang, D. D., Wang, Z., Liu, Y., Qiao, X., Guo, Y., Tian, L., Zheng, P., Xu, Z., Li, Y., Xu, Z., Qi, X., Sun, P., Wang, J., Zheng, F., Li, X., Yin, R., Dallenbach, K. R., Bianchi, F., Petäjä, T., Zhang, Y., Wang, M., Schervish, M., Wang, S., Qiao, L., Wang, Q., Zhou, M., Wang, H., Yu, C., Yao, D., Guo, H., Ye, P., Lee, S., Li, Y. J., Liu, Y., Chi, X., Kerminen, V.-M., Ehn, M., Donahue, N. M., Wang, T., Huang, C., Kulmala, M., Worsnop, D., Jiang, J., and Ding, A.: Secondary organic aerosol formed by condensing anthropogenic vapours over China's megacities, Nat. Geosci., 15, 255–261, https://doi.org/10.1038/s41561-022-00922-5, 2022.

O'Dowd, C. D., Aalto, P., Hmeri, K., Kulmala, M., and Hoffmann, T.: Atmospheric particles from organic vapours, Nature, 416, 497–498, https://doi.org/10.1038/416497a, 2002.

Orlando, J. J. and Tyndall, G. S.: Laboratory studies of organic peroxy radical chemistry: an overview with emphasis on recent issues of atmospheric significance, Chem. Soc. Rev., 41, 6294–6317, https://doi.org/10.1039/C2CS35166H, 2012.

Pan, S. and Wang, L.: Atmospheric Oxidation Mechanism of m-Xylene Initiated by OH Radical, J. Phys. Chem. A, 118, 10778–10787, https://doi.org/10.1021/jp506815v, 2014.

Panopoulou, A., Liakakou, E., Sauvage, S., Gros, V., Locoge, N., Stavroulas, I., Bonsang, B., Gerasopoulos, E., and Mihalopoulos, N.: Yearlong measurements of monoterpenes and isoprene in a Mediterranean city (Athens): Natural vs anthropogenic origin, Atmos. Environ., 243, 117803, https://doi.org/10.1016/j.atmosenv.2020.117803, 2020.

Riccobono, F., Schobesberger, S., Scott, C., Dommen, J., Ortega, I., Rondo, L., Almeida, J., Amorim, A., Bianchi, F., Breitenlechner, M., David, A., Downard, A., Dunne, E., Duplissy, J., Ehrhart, S., Flagan, R., Franchin, A., Hansel, A., Junninen, H., and Baltensperger, U.: Oxidation Products of Biogenic Emissions Contribute to Nucleation of Atmospheric Particles, Science, 344, 717–721, https://doi.org/10.1126/science.1243527, 2014.

Riedel, T. P., Lin, Y.-H., Budisulistiorini, S. H., Gaston, C. J., Thornton, J. A., Zhang, Z., Vizuete, W., Gold, A., and Surratt, J. D.: Heterogeneous Reactions of Isoprene-Derived Epoxides: Reaction Probabilities and Molar Secondary Organic Aerosol Yield Estimates, Environ. Sci. Technol. Lett., 2, 38–42, https://doi.org/10.1021/ez500406f, 2015.

Riva, M., Rantala, P., Krechmer, J. E., Peräkylä, O., Zhang, Y., Heikkinen, L., Garmash, O., Yan, C., Kulmala, M., Worsnop, D., and Ehn, M.: Evaluating the performance of five different chemical ionization techniques for detecting gaseous oxygenated organic species, Atmos. Meas. Tech., 12, 2403–2421, https://doi.org/10.5194/amt-12-2403-2019, 2019.

Roldin, P., Ehn, M., Kurtén, T., Olenius, T., Rissanen, M. P., Sarnela, N., Elm, J., Rantala, P., Hao, L., Hyttinen, N., Heikkinen, L., Worsnop, D. R., Pichelstorfer, L., Xavier, C., Clusius, P., Öström, E., Petäjä, T., Kulmala, M., Vehkamäki, H., Virtanen, A., Riipinen, I., and Boy, M.: The role of highly oxygenated organic molecules in the Boreal aerosol-cloud-climate system, Nat. Commun., 10, 4370, https://doi.org/10.1038/s41467-019-12338-8, 2019.

Rose, C., Zha, Q., Dada, L., Yan, C., Lehtipalo, K., Junninen, H., Mazon, S. B., Jokinen, T., Sarnela, N., Sipilä, M., Petäjä, T., Kerminen, V.-M., Bianchi, F., and Kulmala, M.: Observations of biogenic ion-induced cluster formation in the atmosphere, Sci. Adv., 4, eaar5218, https://doi.org/10.1126/sciadv.aar5218, 2018.

Schervish, M. and Donahue, N. M.: Peroxy radical chemistry and the volatility basis set, Atmos. Chem. Phys., 20, 1183–1199, https://doi.org/10.5194/acp-20-1183-2020, 2020.

Schobesberger, S., Junninen, H., Bianchi, F., Lönn, G., Ehn, M., Lehtipalo, K., Dommen, J., Ehrhart, S., Ortega, I. K., Franchin, A., Nieminen, T., Riccobono, F., Hutterli, M., Duplissy, J., Almeida, J., Amorim, A., Breitenlechner, M., Downard, A. J., Dunne, E. M., Flagan, R. C., Kajos, M., Keskinen, H., Kirkby, J., Kupc, A., Kürten, A., Kurtén, T., Laaksonen, A., Mathot, S., Onnela, A., Praplan, A. P., Rondo, L., Santos, F. D., Schallhart, S., Schnitzhofer, R., Sipilä, M., Tomé, A., Tsagkogeorgas, G., Vehkamäki, H., Wimmer, D., Baltensperger, U., Carslaw, K. S., Curtius, J., Hansel, A., Petäjä, T., Kulmala, M., Donahue, N. M., and Worsnop, D. R.: Molecular understanding of atmospheric particle formation from sulfuric acid and large oxidized organic molecules, P. Natl. Acad. Sci. USA, 110, 17223, https://doi.org/10.1073/pnas.1306973110, 2013.

Seinfeld, J. H. and Pandis, S. N.: Atmospheric chemistry and physics: from air pollution to climate change, John Wiley & Sons, ISBN 9781119221166, 2016.

Song, K., Guo, S., Wang, H., Yu, Y., Wang, H., Tang, R., Xia, S., Gong, Y., Wan, Z., Lv, D., Tan, R., Zhu, W., Shen, R., Li, X., Yu, X., Chen, S., Zeng, L., and Huang, X.: Measurement report: Online measurement of gas-phase nitrated phenols utilizing a CI-LToF-MS: primary sources and secondary formation, Atmos. Chem. Phys., 21, 7917–7932, https://doi.org/10.5194/acp-21-7917-2021, 2021.

Stocker, T.: Climate change 2013: the physical science basis: Working Group I contribution to the Fifth assessment report of the Intergovernmental Panel on Climate Change, Cambridge University Press, Cambridge, New York, https://www.ipcc.ch/report/ar5/wg1/ (last access: 3 August 2022), 2014.

Stolzenburg, D., Fischer, L., Vogel, A. L., Heinritzi, M., Schervish, M., Simon, M., Wagner, A. C., Dada, L., Ahonen, L. R., Amorim, A., Baccarini, A., Bauer, P. S., Baumgartner, B., Bergen, A., Bianchi, F., Breitenlechner, M., Brilke, S., Buenrostro Mazon,

S., Chen, D., Dias, A., Draper, D. C., Duplissy, J., El Haddad, I., Finkenzeller, H., Frege, C., Fuchs, C., Garmash, O., Gordon, H., He, X., Helm, J., Hofbauer, V., Hoyle, C. R., Kim, C., Kirkby, J., Kontkanen, J., Kürten, A., Lampilahti, J., Lawler, M., Lehtipalo, K., Leiminger, M., Mai, H., Mathot, S., Mentler, B., Molteni, U., Nie, W., Nieminen, T., Nowak, J. B., Ojdanic, A., Onnela, A., Passananti, M., Petäjä, T., Quéléver, L. L. J., Rissanen, M. P., Sarnela, N., Schallhart, S., Tauber, C., Tomé, A., Wagner, R., Wang, M., Weitz, L., Wimmer, D., Xiao, M., Yan, C., Ye, P., Zha, Q., Baltensperger, U., Curtius, J., Dommen, J., Flagan, R. C., Kulmala, M., Smith, J. N., Worsnop, D. R., Hansel, A., Donahue, N. M., and Winkler, P. M.: Rapid growth of organic aerosol nanoparticles over a wide tropospheric temperature range, P. Natl. Acad. Sci. USA, 115, 9122, https://doi.org/10.1073/pnas.1807604115, 2018.

Tan, Q., Ge, B., Xu, X., Gan, L., Yang, W., Chen, X., Pan, X., Wang, W., Li, J., and Wang, Z.: Increasing impacts of the relative contributions of regional transport on air pollution in Beijing: Observational evidence, Environ. Pollut., 292, 118407, https://doi.org/10.1016/j.envpol.2021.118407, 2022.

Teng, A. P., Crounse, J. D., and Wennberg, P. O.: Isoprene Peroxy Radical Dynamics, J. Am. Chem. Soc., 139, 5367–5377, https://doi.org/10.1021/jacs.6b12838, 2017.

Tröstl, J., Chuang, W. K., Gordon, H., Heinritzi, M., Yan, C., Molteni, U., Ahlm, L., Frege, C., Bianchi, F., Wagner, R., Simon, M., Lehtipalo, K., Williamson, C., Craven, J. S., Duplissy, J., Adamov, A., Almeida, J., Bernhammer, A.-K., Breitenlechner, M., Brilke, S., Dias, A., Ehrhart, S., Flagan, R. C., Franchin, A., Fuchs, C., Guida, R., Gysel, M., Hansel, A., Hoyle, C. R., Jokinen, T., Junninen, H., Kangasluoma, J., Keskinen, H., Kim, J., Krapf, M., Kürten, A., Laaksonen, A., Lawler, M., Leiminger, M., Mathot, S., Möhler, O., Nieminen, T., Onnela, A., Petäjä, T., Piel, F. M., Miettinen, P., Rissanen, M. P., Rondo, L., Sarnela, N., Schobesberger, S., Sengupta, K., Sipilä, M., Smith, J. N., Steiner, G., Tomè, A., Virtanen, A., Wagner, A. C., Weingartner, E., Wimmer, D., Winkler, P. M., Ye, P., Carslaw, K. S., Curtius, J., Dommen, J., Kirkby, J., Kulmala, M., Riipinen, I., Worsnop, D. R., Donahue, N. M., and Baltensperger, U.: The role of low-volatility organic compounds in initial particle growth in the atmosphere, Nature, 533, 527–531, https://doi.org/10.1038/nature18271, 2016.

Wagner, P. and Kuttler, W.: Biogenic and anthropogenic isoprene in the near-surface urban atmosphere – A case study in Essen, Germany, Sci. Total Environ., 475, 104–115, https://doi.org/10.1016/j.scitotenv.2013.12.026, 2014.

Wang, H., Lu, K., Guo, S., Wu, Z., Shang, D., Tan, Z., Wang, Y., Le Breton, M., Lou, S., Tang, M., Wu, Y., Zhu, W., Zheng, J., Zeng, L., Hallquist, M., Hu, M., and Zhang, Y.: Efficient N_2O_5 uptake and NO_3 oxidation in the outflow of urban Beijing, Atmos. Chem. Phys., 18, 9705–9721, https://doi.org/10.5194/acp-18-9705-2018, 2018.

Wang, L., Liu, Z., Sun, Y., Ji, D., and Wang, Y.: Long-range transport and regional sources of $PM_{2.5}$ in Beijing based on long-term observations from 2005 to 2010, Atmos. Res., 157, 37–48, https://doi.org/10.1016/j.atmosres.2014.12.003, 2015.

Wang, S., Wu, R., Berndt, T., Ehn, M., and Wang, L.: Formation of Highly Oxidized Radicals and Multifunctional Products from the Atmospheric Oxidation of Alkylbenzenes, Environmental Science & Technology, 51, 8442-8449, 10.1021/acs.est.7b02374, 2017.

Wang, S., Riva, M., Yan, C., Ehn, M., and Wang, L.: Primary Formation of Highly Oxidized Multifunctional Products in the OH-Initiated Oxidation of Isoprene: A Combined Theoretical and Experimental Study, Environ. Sci. Technol., 52, 12255–12264, https://doi.org/10.1021/acs.est.8b02783, 2018.

Wang, Y., Hu, M., Wang, Y., Zheng, J., Shang, D., Yang, Y., Liu, Y., Li, X., Tang, R., Zhu, W., Du, Z., Wu, Y., Guo, S., Wu, Z., Lou, S., Hallquist, M., and Yu, J. Z.: The formation of nitro-aromatic compounds under high NO_x and anthropogenic VOC conditions in urban Beijing, China, Atmos. Chem. Phys., 19, 7649–7665, https://doi.org/10.5194/acp-19-7649-2019, 2019.

Wang, Z., Ehn, M., Rissanen, M. P., Garmash, O., Quéléver, L., Xing, L., Monge-Palacios, M., Rantala, P., Donahue, N. M., Berndt, T., and Sarathy, S. M.: Efficient alkane oxidation under combustion engine and atmospheric conditions, Commun. Chem., 4, 18, https://doi.org/10.1038/s42004-020-00445-3, 2021.

Wu, R., Vereecken, L., Tsiligiannis, E., Kang, S., Albrecht, S. R., Hantschke, L., Zhao, D., Novelli, A., Fuchs, H., Tillmann, R., Hohaus, T., Carlsson, P. T. M., Shenolikar, J., Bernard, F., Crowley, J. N., Fry, J. L., Brownwood, B., Thornton, J. A., Brown, S. S., Kiendler-Scharr, A., Wahner, A., Hallquist, M., and Mentel, T. F.: Molecular composition and volatility of multi-generation products formed from isoprene oxidation by nitrate radical, Atmos. Chem. Phys., 21, 10799–10824, https://doi.org/10.5194/acp-21-10799-2021, 2021.

Xu, L., Møller, K. H., Crounse, J. D., Kjaergaard, H. G., and Wennberg, P. O.: New Insights into the Radical Chemistry and Product Distribution in the OH-Initiated Oxidation of Benzene, Environ. Sci. Technol., 54, 13467–13477, https://doi.org/10.1021/acs.est.0c04780, 2020.

Xu, Z. N., Nie, W., Liu, Y. L., Sun, P., Huang, D. D., Yan, C., Krechmer, J., Ye, P. L., Xu, Z., Qi, X. M., Zhu, C. J., Li, Y. Y., Wang, T. Y., Wang, L., Huang, X., Tang, R. Z., Guo, S., Xiu, G. L., Fu, Q. Y., Worsnop, D., Chi, X. G., and Ding, A. J.: Multifunctional Products of Isoprene Oxidation in Polluted Atmosphere and Their Contribution to SOA, Geophys. Res. Lett., 48, e2020GL089276, https://doi.org/10.1029/2020GL089276, 2021.

Yan, C., Nie, W., Äijälä, M., Rissanen, M. P., Canagaratna, M. R., Massoli, P., Junninen, H., Jokinen, T., Sarnela, N., Häme, S. A. K., Schobesberger, S., Canonaco, F., Yao, L., Prévôt, A. S. H., Petäjä, T., Kulmala, M., Sipilä, M., Worsnop, D. R., and Ehn, M.: Source characterization of highly oxidized multifunctional compounds in a boreal forest environment using positive matrix factorization, Atmos. Chem. Phys., 16, 12715–12731, https://doi.org/10.5194/acp-16-12715-2016, 2016.

Yan, C., Nie, W., Vogel, A. L., Dada, L., Lehtipalo, K., Stolzenburg, D., Wagner, R., Rissanen, M. P., Xiao, M., Ahonen, L., Fischer, L., Rose, C., Bianchi, F., Gordon, H., Simon, M., Heinritzi, M., Garmash, O., Roldin, P., Dias, A., Ye, P., Hofbauer, V., Amorim, A., Bauer, P. S., Bergen, A., Bernhammer, A. K., Breitenlechner, M., Brilke, S., Buchholz, A., Mazon, S. B., Canagaratna, M. R., Chen, X., Ding, A., Dommen, J., Draper, D. C., Duplissy, J., Frege, C., Heyn, C., Guida, R., Hakala, J., Heikkinen, L., Hoyle, C. R., Jokinen, T., Kangasluoma, J., Kirkby, J., Kontkanen, J., Kürten, A., Lawler, M. J., Mai, H., Mathot, S., Mauldin, R. L., Molteni, U., Nichman, L., Nieminen, T., Nowak, J., Ojdanic, A.,

Onnela, A., Pajunoja, A., Petäjä, T., Piel, F., Quéléver, L. L. J., Sarnela, N., Schallhart, S., Sengupta, K., Sipilä, M., Tomé, A., Tröstl, J., Väisänen, O., Wagner, A. C., Ylisirniö, A., Zha, Q., Baltensperger, U., Carslaw, K. S., Curtius, J., Flagan, R. C., Hansel, A., Riipinen, I., Smith, J. N., Virtanen, A., Winkler, P. M., Donahue, N. M., Kerminen, V. M., Kulmala, M., Ehn, M., and Worsnop, D. R.: Size-dependent influence of NO_x on the growth rates of organic aerosol particles, Sci. Adv., 6, eaay4945, https://doi.org/10.1126/sciadv.aay4945, 2020.

Yan, C., Yin, R., Lu, Y., Dada, L., Yang, D., Fu, Y., Kontkanen, J., Deng, C., Garmash, O., Ruan, J., Baalbaki, R., Schervish, M., Cai, R., Bloss, M., Chan, T., Chen, T., Chen, Q., Chen, X., Chen, Y., Chu, B., Dällenbach, K., Foreback, B., He, X., Heikkinen, L., Jokinen, T., Junninen, H., Kangasluoma, J., Kokkonen, T., Kurppa, M., Lehtipalo, K., Li, H., Li, H., Li, X., Liu, Y., Ma, Q., Paasonen, P., Rantala, P., Pileci, R. E., Rusanen, A., Sarnela, N., Simonen, P., Wang, S., Wang, W., Wang, Y., Xue, M., Yang, G., Yao, L., Zhou, Y., Kujansuu, J., Petäjä, T., Nie, W., Ma, Y., Ge, M., He, H., Donahue, N. M., Worsnop, D. R., Veli-Matti, K., Wang, L., Liu, Y., Zheng, J., Kulmala, M., Jiang, J., and Bianchi, F.: The Synergistic Role of Sulfuric Acid, Bases, and Oxidized Organics Governing New-Particle Formation in Beijing, Geophys. Res. Lett., 48, e2020GL091944, https://doi.org/10.1029/2020GL091944, 2021.

Ye, C., Yuan, B., Lin, Y., Wang, Z., Hu, W., Li, T., Chen, W., Wu, C., Wang, C., Huang, S., Qi, J., Wang, B., Wang, C., Song, W., Wang, X., Zheng, E., Krechmer, J. E., Ye, P., Zhang, Z., Wang, X., Worsnop, D. R., and Shao, M.: Chemical characterization of oxygenated organic compounds in the gas phase and particle phase using iodide CIMS with FIGAERO in urban air, Atmos. Chem. Phys., 21, 8455–8478, https://doi.org/10.5194/acp-21-8455-2021, 2021.

Zaytsev, A., Koss, A. R., Breitenlechner, M., Krechmer, J. E., Nihill, K. J., Lim, C. Y., Rowe, J. C., Cox, J. L., Moss, J., Roscioli, J. R., Canagaratna, M. R., Worsnop, D. R., Kroll, J. H., and Keutsch, F. N.: Mechanistic study of the formation of ring-retaining and ring-opening products from the oxidation of aromatic compounds under urban atmospheric conditions, Atmos. Chem. Phys., 19, 15117–15129, https://doi.org/10.5194/acp-19-15117-2019, 2019.

Zha, Q., Yan, C., Junninen, H., Riva, M., Sarnela, N., Aalto, J., Quéléver, L., Schallhart, S., Dada, L., Heikkinen, L., Peräkylä, O., Zou, J., Rose, C., Wang, Y., Mammarella, I., Katul, G., Vesala, T., Worsnop, D. R., Kulmala, M., Petäjä, T., Bianchi, F., and Ehn, M.: Vertical characterization of highly oxygenated molecules (HOMs) below and above a boreal forest canopy, Atmos. Chem. Phys., 18, 17437–17450, https://doi.org/10.5194/acp-18-17437-2018, 2018.

Zhang, H., Li, H., Zhang, Q., Zhang, Y., Zhang, W., Wang, X., Bi, F., Chai, F., Gao, J., Meng, L., Yang, T., Chen, Y., Cheng, Q., and Xia, F.: Atmospheric Volatile Organic Compounds in a Typical Urban Area of Beijing: Pollution Characterization, Health Risk Assessment and Source Apportionment, Atmosphere, 8, 61, https://doi.org/10.3390/atmos8030061, 2017.

Zhang, H., Zhang, Y., Huang, Z., Acton, W. J. F., Wang, Z., Nemitz, E., Langford, B., Mullinger, N., Davison, B., Shi, Z., Liu, D., Song, W., Yang, W., Zeng, J., Wu, Z., Fu, P., Zhang, Q., and Wang, X.: Vertical profiles of biogenic volatile organic compounds as observed online at a tower in Beijing, J. Environ. Sci., 95, 33-42, https://doi.org/10.1016/j.jes.2020.03.032, 2020.

Zhang, Q., Jimenez, J. L., Canagaratna, M. R., Allan, J. D., Coe, H., Ulbrich, I., Alfarra, M. R., Takami, A., Middlebrook, A. M., Sun, Y. L., Dzepina, K., Dunlea, E., Docherty, K., DeCarlo, P. F., Salcedo, D., Onasch, T., Jayne, J. T., Miyoshi, T., Shimono, A., Hatakeyama, S., Takegawa, N., Kondo, Y., Schneider, J., Drewnick, F., Borrmann, S., Weimer, S., Demerjian, K., Williams, P., Bower, K., Bahreini, R., Cottrell, L., Griffin, R. J., Rautiainen, J., Sun, J. Y., Zhang, Y. M., and Worsnop, D. R.: Ubiquity and dominance of oxygenated species in organic aerosols in anthropogenically-influenced Northern Hemisphere midlatitudes, Geophys. Res. Lett., 34, L13801, https://doi.org/10.1029/2007GL029979, 2007.

Zhang, Y., Peräkylä, O., Yan, C., Heikkinen, L., Äijälä, M., Daellenbach, K. R., Zha, Q., Riva, M., Garmash, O., Junninen, H., Paatero, P., Worsnop, D., and Ehn, M.: A novel approach for simple statistical analysis of high-resolution mass spectra, Atmos. Meas. Tech., 12, 3761–3776, https://doi.org/10.5194/amt-12-3761-2019, 2019.

Zhang, Y.-Q., Ding, X., He, Q.-F., Wen, T.-X., Wang, J.-Q., Yang, K., Jiang, H., Cheng, Q., Liu, P., Wang, Z.-R., He, Y.-F., Hu, W.-W., Wang, Q.-Y., Xin, J.-Y., Wang, Y.-S., and Wang, X.-M.: Observational Insights into Isoprene Secondary Organic Aerosol Formation through the Epoxide Pathway at Three Urban Sites from Northern to Southern China, Environ. Sci. Technol., 56, 4795–4805, https://doi.org/10.1021/acs.est.1c06974, 2022.

Zhao, Y., Thornton, J. A., and Pye, H. O. T.: Quantitative constraints on autoxidation and dimer formation from direct probing of monoterpene-derived peroxy radical chemistry, P. Natl. Acad. Sci. USA, 115, 12142, https://doi.org/10.1073/pnas.1812147115, 2018.